

Thesis  
2957

University of Nevada

Reno

✓  
Aquifer Storage Characteristics  
of Paleozoic Carbonate Rocks in Southeastern Nevada  
Estimated from Harmonic Analysis of Water-Level Fluctuations

A dissertation submitted in partial fulfillment of the  
requirements for the degree of  
Doctor of Philosophy in Hydrology

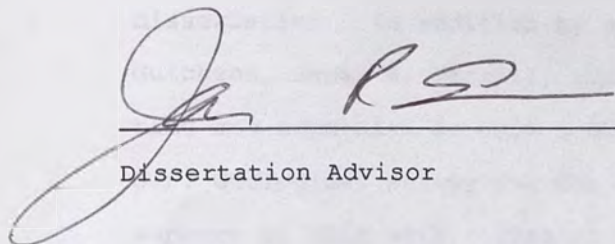
by

Kathryn Carmille Kilroy

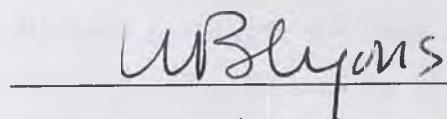
|||

May, 1992

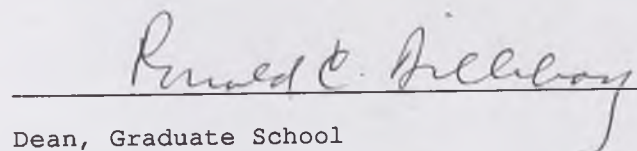
The dissertation of Kathryn Carmille Kilroy is approved:



Dissertation Advisor



Department Chair



Dean, Graduate School

University of Nevada

Reno

May 1992

**ACKNOWLEDGEMENTS**

I wish to extend my sincerest appreciation to my committee Chair James Carr and principal advisor Clint Case, both of whom contributed significant moral and technical support to the betterment of this dissertation. In addition my committee members Fred Gifford, Jon Guichens, James R. Harrill, and Bob Merrill, all of whom gave of their time and expertise in this endeavor. Thanks are also extended to the U.S. Geological Survey for the use of their data, and funding in support of this work. Special thanks go to USGS employees Devin Galloway and Paul Hsieh for providing additional review comments, to Michael Dettinger for help in conceiving this project, and to Lori Carpenter for data entry assistance.

**ABSTRACT**

The Paleozoic carbonate-rock aquifers of southeastern Nevada have significant secondary porosity due to fractures and solution cavities. Measured aquifer transmissivities are moderate to high ( $1.2 \times 10^{-5}$  to  $5.3 \times 10^{-1} \text{ m}^2 \text{ s}^{-1}$ ); however, only limited information is available on the storage characteristics of these aquifers.

This paper reviews the one- and three-dimensional theories of aquifer dilatation due to earth tides, which may be used to determine storage characteristics. The three-dimensional theory includes a term to accommodate compressible grains and this concept is extended in this paper to the one-dimensional theory. Porosity is determined from specific storage and aquifer response to barometric fluctuations, and a correction for degree of confinement is applied. Aquifer matrix compressibility is determined by an iterative process from specific storage and porosity. Methods of data collection, analysis, and results are presented.

Water-level records for eleven wells and one open fault that penetrate the carbonate-rock aquifers and one well in alluvium were analyzed. Estimates of specific storage for the carbonate rock aquifers range from  $1.50 \times 10^{-7}$  to  $3.47 \times 10^{-7} \text{ m}^{-1}$  and average  $2.1 \times 10^{-7} \text{ m}^{-1}$ . Storage coefficient ranges from  $6.3 \times 10^{-6}$  to  $1.21 \times 10^{-4}$ . Porosity ranges from 1.0 to 4.4 percent and averages 1.9 percent. Matrix compressibility ranges from  $1.05 \times 10^{-11}$  to  $1.35 \times 10^{-11} \text{ Pa}^{-1}$  and averages  $1.15 \times 10^{-11} \text{ Pa}^{-1}$ .

CONTENTS

	page
Introduction-----	1
Purpose and scope-----	2
Previous work-----	2
Review of aquifer-dilatation theory-----	4
Aquifer dilatation-----	4
Earth-tide dilatation-----	4
Barometric dilatation-----	7
Barometric efficiency-----	8
Phase Effects-----	10
Earth tide dilatation-----	12
Global theory-----	12
Soil mechanics theory-----	17
Specific storage-----	18
Specific storage in terms of aquifer dilatation-----	20
Porosity-----	21
Aquifer matrix compressibility-----	22
Methods of investigation-----	23
Data collection-----	25
Filtering-----	28
Barometric efficiency-----	31
Harmonic analysis-----	42
Instrumentation-----	44
Pressure transducers-----	44
Floats-----	46
Barometric pressure-----	46
Aquifer storage characteristics-----	48
Estimated parameters-----	50
Measured parameters-----	51
Calculated parameters-----	53

Matrix compressibility-----	55
Specific storage-----	55
Storage coefficient-----	58
Porosity-global theory-----	58
Porosity-soil mechanics theory-----	61
Conclusions-----	62
References cited-----	65
Notation-----	70
Appendicies-----	73
Appendix A neutron-density estimation of porosity-----	73
Appendix B acoustic density estimation of porosity-----	74

#### ILLUSTRATIONS

Figure 1. Stress configuration and water-level response to A. earth tide; B. barometric pressure-----	6
2. Water level fluctuations at Devils Hole, Nevada-----	9
3. Configuration of the diurnal, O1 and K1 and semidiurnal M2, N2, and S2 earth tides-----	16
4. Harmonic-analysis algorithm-----	24
5. Aperiodic barometric-pressure head against aperiodic water level at Devils Hole, Nevada-----	32
6. Barometric efficiency at Devils Hole, Nevada-----	33
7. Relation between barometric efficiency and frequency at which it is calculated for a well in a partially confined aquifer-----	35
8. Location of study sites, shaded area indicates area of carbonate rock aquifer-----	37
9. Barometric efficiency as a function of frequency-----	40
10. Neutron-density cross plot for seven zones of well CE-DT-4-----	75
11. Accoustic-density cross plot for seven zones of well CE-DT-4-----	76

## TABLES

Table 1.	Constants used in calculation of tide-generation potential (W2)-----	13
2.	Constants used in this paper-----	15
3.	Well or site locations, specifications, and instrumentation details-----	45
4.	Geologic characteristics of the study sites-----	49
5.	Harmonic-analysis results using an assumed value of $\alpha^* = .32$ -----	52
6.	Estimated porosity and matrix compressibility based on an assumption of $\alpha^* = .32$ -----	54
7.	Revised storage characteristics based on new estimates of matrix compressibility showing porosity estimates from borehole geophysical studies for comparison-----	56

**AQUIFER STORAGE CHARACTERISTICS OF  
PALEOZOIC CARBONATE ROCKS IN SOUTHEASTERN NEVADA  
ESTIMATED FROM HARMONIC ANALYSIS OF WATER-LEVEL FLUCTUATIONS**

By Kathryn C. Kilroy

**INTRODUCTION**

Specific storage is a difficult aquifer property to determine accurately because of the insensitivity of hydraulic-test analysis of wells to storativity. An order-of-magnitude estimate of specific storage satisfies the accuracy requirements of many ground-water-hydraulics problems. These estimates are often made using knowledge of geologic characteristics such as grain size or rock type. For those applications where a more accurate estimate is necessary, only three measurement methods are available: (1) pumping/injection tests using observation wells; (2) geophysical neutron-density and acoustic-density analyses; and (3) harmonic analysis of water-level fluctuations due to earth tides. Each of these methods has drawbacks that may render it unsuitable for a particular study. Pumping tests require more than one well, can be expensive, and may not be feasible for remote well sites. Geophysical logging is expensive, must be carried out prior to casing the hole, and is not done routinely.

A full analysis of aquifer storage characteristics can be accomplished only if the well responds to both earth tides and barometric pressure fluctuations and if hourly water-level measurements can be made and recorded for a period of approximately 2 months or more. Because harmonic analysis and geophysical methods do not require removal of water from the well, they are particularly appropriate where contamination is a problem.

### Purpose and Scope

The purpose of this paper is to review the one- and three-dimensional theories of earth-tide dilatation and the assumptions made in their use; discuss the use of a term for compressible grains that appears in the three-dimensional equation, and show how it can be applied to the one-dimensional equation; describe the methods of data collection and reduction for harmonic analysis used in this study; and present aquifer storage characteristics and matrix compressibility for study sites in the Paleozoic carbonate aquifers of southeastern Nevada. This paper includes tables of all required constants except those that must be measured for a particular site. Post-1967 values of tidal coefficients are presented.

### Previous Work

Water-level fluctuations that correspond to earth-tide frequencies have been observed in wells for over 100 years. Melchior (1960) recognized the usefulness of these fluctuations in determining aquifer parameters. Using the concept of an aquifer as a finite cavity, he described tidal dilatation in terms of lunisolar tide-generation potential, Poisson's ratio, and the Love numbers. Bredehoeft (1967) carries the concept a step further by relating the aquifer dilatation to specific storage, a term defined by Jacob (1940). Bredehoeft also shows that the finite cavity concept was limited in scope and introduces a porosity term into his basic equations. Carr and Van der Kamp (1969) calculate aquifer specific storage from sea tides in coastal areas. Bodvarsson (1970) points out the importance of inertial terms in computations of specific storage in fractured rocks. Robinson and Bell (1971) also work with ocean tides; they use ratios of tidal constituents to calculate porosity. Rhoades and Robinson (1979) show that removal of the barometric effect prior to harmonic analysis yields higher quality estimates of specific storage and porosity.

Many investigators (Narasimhan and others, 1984, p.1915) discuss the importance of measuring strain directly in the aquifer, separately from fluid-pressure changes, in order to reduce the potential errors caused by the application of the calculated homogeneous strain tide.

Several authors have worked on the general formulation of poroelastic problems. Biot (1941) presents a three-dimensional expression for the change in pressure head during compaction. This approach includes terms for instantaneous and final compressibility. Using Biot's formulation, Nur and Byerlee (1971) develop an effective-stress law for elastic strain that includes the more commonly encountered terms, grain and matrix compressibility. Carroll (1979) does the same thing for anisotropic elastic deformation. Rice and Cleary (1976) also work on the interaction of stress and fluid pressure in porous media. Van der Kamp and Gale (1983) show that the assumption of incompressible grains may lead to overestimation of parameters, particularly for fractured media.

Some authors have analyzed water-level response to earth tides where drainage effects are evident. Hsieh and others (1987) present a technique for estimating aquifer transmissivity from earth-tide-induced fluctuations of water levels in artesian wells when well-bore storage effects are significant. Rojstaczer (1988A) presents methods for correcting the measured strain sensitivity of water-level responses to earth tides when the well response to atmospheric loading indicates the occurrence of water-table drainage at earth-tide frequencies.

Several other papers may be of interest. Marine (1975), Bower (1983), and Hanson (1984) use earth-tide analysis in evaluating fractured rocks. Clark (1967) provides a method for computing the barometric efficiency of a well. Gilliland (1969) describes the rigid-plate model for the barometric effect on a confined aquifer, and Weeks (1979) discusses the barometric effect on an unconfined aquifer.

## REVIEW OF AQUIFER-DILATATION THEORY

Two different means of estimating aquifer-dilatation have been developed in the literature. One is based on global estimates of earth-tide dilatation and the other is based on local soil mechanics properties. The global theory is presented under the assumption of incompressible grains and is one-dimensional, and the soil mechanics theory is presented under the assumption that grains may be compressible and is three-dimensional. A synthesis of these two perspectives is presented here including the addition of a term to the global theory to allow for compressible grains. The global theory is based on the works of Jacob (1940), Bredehoeft (1967), and Rhoads and Robinson (1979), whereas the rock-mechanics theory is based on the works of Biot (1941), Nur and Byerlee (1971), Rice and Cleary (1976), and Van der Camp and Gale (1983). Both approaches assume linear elasticity of the aquifer; that is, each component of strain is a linear function of stress. They also assume static conditions (no drainage between the aquifer and either confining units or the well), insignificant well-bore storage effects, and no head loss due to friction in the aquifer.

### Aquifer Dilatation

Dilatation is a change in volume. Aquifer dilatation,  $\Delta a$ , (dimensionless) is the ratio of the change in aquifer volume,  $dV_a$ , to the original aquifer volume,  $V_a$ .

$$\Delta a = \frac{dV_a}{V_a} \quad (1)$$

$V_a$

The aquifer is composed of pores,  $V_p$ , and solids,  $V_s$ .

$$V_a = V_p + V_s \quad (2)$$

Most aquifers have pores that are more compressible than the solid material so that aquifer dilatation causes a change in size of the pores and a concomitant change in pore pressure.

There are several different causes of aquifer dilatation of both tidal and non tidal origin. Water levels in wells tapping confined aquifers may fluctuate in response to seasonal climatic variation, changes in nearby pumping and recharge rates, seismic events, barometric pressure fluctuations, and earth-tide effects. Each of these changes is associated with a characteristic periodicity that may be only minutes long for seismic events, but months long for seasonal effects. In this paper only the effects of earth tides and barometric fluctuations, which have periodicities of approximately 0.5 to 10 days, will be discussed.

#### Earth Tide Dilatation

The earth tide is a dilatation caused by a body force, the slight change in earth's gravitational acceleration as a celestial body, the sun or the moon, passes nearby. Aquifer dilatation caused by the earth tide,  $\Delta e$ , causes a change in pore pressure,  $\rho g \Delta h_a$ , that is directly communicated to the well bore as a change in head,  $\Delta h_w$ . See figure 1a.

$$\Delta h_a = \Delta h_w. \quad (3)$$

The angle,  $\phi_e$ , between the earth-tide dilatation,  $\Delta e$ , and the water-level response is theoretically  $0.0^\circ$ , however the two may not be in phase if the aquifer has low hydraulic conductivity, there is poor interaction between the well aquifer system, or if the aquifer does not dilate evenly. A dilatometer is required to measure the earth-tide dilatation. Dilatometers are expensive and difficult to install and for this reason,  $\phi_e$  is often assumed to be  $0.0^\circ$ . Rhoads and Robinson (1979, p.6078) suggest that a correction may be applied to the computations if  $\phi_e$  is known.

$$\Delta e^* = \Delta e \cos \phi_e. \quad (4)$$

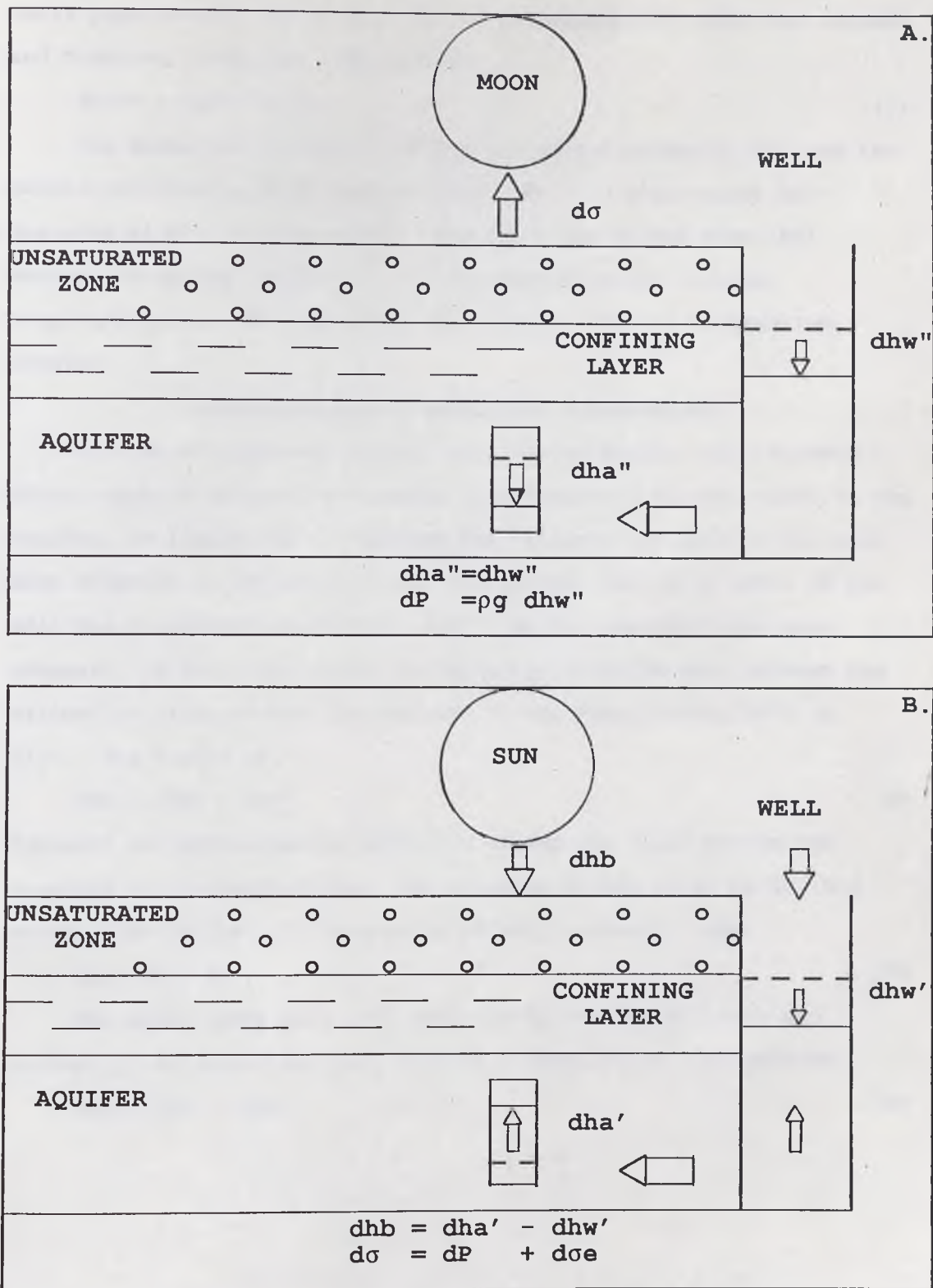


Figure 1.--Stress configuration and water-level response to:  
 A. earth tide; B. barometric pressure.

Small phase shifts can be handled with trigonometric functions (Rhoads and Robinson, 1979, eqn. 29, p.6074):

$$dhw''^* = dhw'' \cos \phi_w'' \quad (5)$$

The angle,  $\phi_t$ , between the tide generation potential  $W_2$ , and the earth-tide dilatation is theoretically  $180^\circ$  but also cannot be measured without a dilatometer. The phase may differ from  $180^\circ$  because of aquifer geometry or anisotropy of aquifer matrix compressibility. The sum of the two angles,  $\phi_w''$  can be measured, however.

#### Dilatation Due to Barometric Fluctuations

Barometric pressure,  $p_g$   $d_{hb}$ , acts on the aquifer as a surface force, some of which is attenuated by compression of the solids in the aquifer, or leakage of air through the aquifer, and acts in the well bore directly on the water level. Therefore, the water level in the well due to barometric effects,  $d_{hw}'$  does not represent the pore pressure,  $p_g$   $d_{ha}'$ , but rather it reflects the difference between the barometric pressure and the pressure in the pores (Bear, 1972, p. 211). See figure 1b.

$$d_{hb} = d_{ha}' - d_{hw}' \quad (6)$$

Equation (4) parallels the effective stress law where barometric pressure is the total stress,  $d\sigma$ , pressure in the pores is  $dP$ , and water level in the well represents effective stress,  $-d\sigma_e$ .

$$d\sigma = dP + d\sigma_e. \quad (7)$$

The water level in a well affected by both earth tides and barometric fluctuations,  $d_{hw}$ , will be a function of both effects.

$$d_{hw} = d_{hw}' + d_{hw}'' \quad (8)$$

Most of the barometric pressure signal occurs at longer periods than the earth tide, however the diurnal earth tide is very close in period to barometric fluctuations caused by daily solar heating of the atmosphere. For this reason pore-pressure changes in an aquifer due to earth tides cannot be measured directly in an open well influenced by barometric pressure, and it cannot be separated from the total water level signal by frequency methods alone. Instead, the barometric effect must first be determined and then removed from the total water-level signal in order to yield the water-level fluctuations due to earth tides. A simple means of separating the two different frequency components of water level is based on the concept of barometric efficiency.

#### Barometric Efficiency

The barometric efficiency of a well, BE, is the ratio of barometric-pressure-induced variations in water level observed in the well, to variations in atmospheric-pressure head (Jacob, 1940, p. 575):

$$BE = \frac{-dhw'}{dhw} \quad (9)$$

This may also be written in terms of stress as:

$$BE = \frac{d\sigma_e}{d\sigma} \quad (10)$$

Rearranging equation (6 & 8) and substituting equation (8) into equation (6) yields

$$dhw'' = dhw + BE dhw \quad (11)$$

An example of water-level fluctuations due to both earth tides and barometric pressure changes is shown in figure 2a and 2b. Figure 2c shows the water-level fluctuations due only to earth tides after application of equation (11).

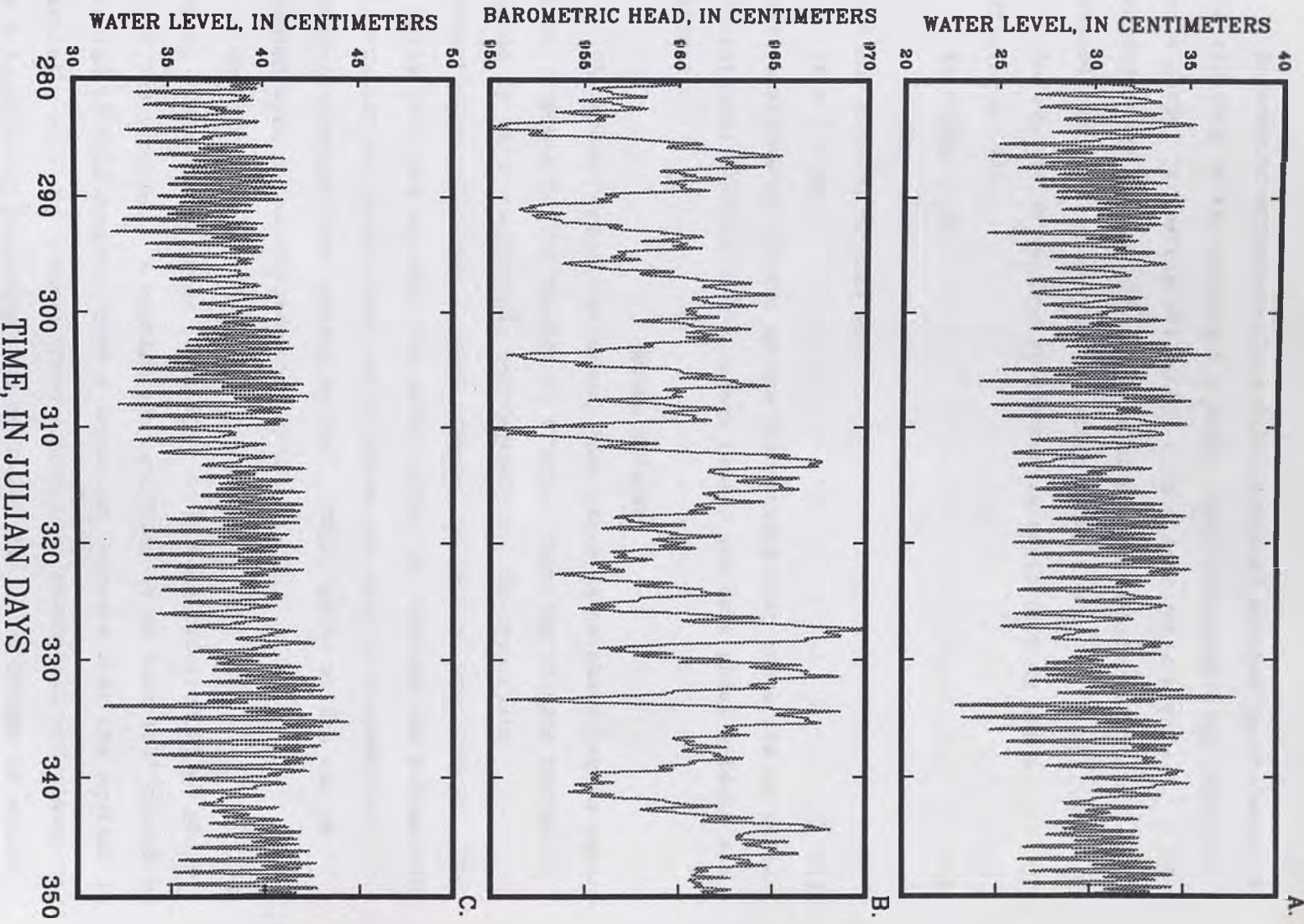


Figure 2.-- Water-level fluctuations at Devils Hole Nevada,  
A. Raw water-level data showing earth-tide and barometric effects,  
B. Barometric pressure data showing daily and longer cyclicity,  
C. Water-level fluctuations due to earth tides.

Barometric efficiency in a fully confined aquifer is an index of the rigidity of the aquifer. A rigid (low-compressibility) aquifer has a larger barometric efficiency than a soft (more highly compressible) aquifer because more of the barometric effect is transmitted to the pores by the rigid material.

An expression related to barometric efficiency is tidal efficiency, TE,

$$TE = \frac{dha'}{dhb} = \frac{dP}{d\sigma} \quad (12)$$

This may also be written as:

$$TE = 1 - BE. \quad (13)$$

This relationship depends on the assumptions that there are no other dilatational effects such as ocean tides, and that phase effects are minimal.

#### Phase Effects

The above derivation assumes that there is no phase lag in water-level response to the barometric effect. Such lag effects may be caused by local topographic heterogeneities, low hydraulic conductivity, well bore storage effects, or partial confinement. For a fully confined aquifer, the phase angle,  $\phi_b$ , between the barometric fluctuation and water-level oscillations due only to barometric pressure changes,  $dhw'$  should be  $180^\circ$ . Small phase shifts can be handled with trigonometric functions.

$$dhw'^* = dhw' \cos \phi_b, \quad (14)$$

where,  $dhw'^*$  is the water level that would have occurred if no phase shift had occurred. A significant deviation of  $\phi_b$  from  $180^\circ$  cannot be handled in this manner. Such a deviation suggests that the aquifer is partially confined. Under these conditions, barometric efficiency may be a function of frequency, and equation (14) is no longer valid.

For a partially confined aquifer, barometric pressure is distributed to the pore water in four ways: (1) atmospheric pressure acts directly on the water in the well bore that is in contact at the well screen with water in the pores, (2) part of the atmospheric-pressure wave moves through the air in the unsaturated zone and acts directly on the water table, (3) part of the atmospheric pressure acts on the rock matrix such that it changes the effective stress, and (4) part of the change in effective stress is transmitted indirectly through the rock fabric (as pores in the rock contract) as an additional stress on the pore water. For such an aquifer, barometric efficiency is a function of matrix rigidity, and the vertical permeability of the semiconfining unit to air.

A partially-confined aquifer responds as a confined aquifer if the barometric changes occur so rapidly that atmospheric pressure waves do not have time to travel through the air in the confining units and act on the water in the aquifer before the pressure wave has acted on the rock matrix. In this case, mechanism (2) is negligible compared to mechanisms (1), (3) and (4). If barometric changes occur slowly enough to allow pressure waves to migrate through the partial confining unit, a lag, and(or) dampening of the response occurs. For a partially confined aquifer, therefore, barometric efficiency must be determined from the high-frequency response of the well where mechanism (2) is negligible (Rojstaczer, 1988A, p. 1931). This is the static-confined barometric efficiency,  $BE'$ . Under such conditions equation (14) may now be written as:

$$BE' = \frac{-dhw'(f)}{dwb(f)}, \quad (15)$$

where,

$dhw'(f)$  is water level fluctuation at a particular frequency due to barometric effects, and

$d_h b(f)$  is barometric pressure head fluctuation at the same frequency.

$$BE' = \frac{-d_h w'(\text{high frequency})}{d_h b(\text{high frequency})} \quad (16)$$

### Earth-Tide Dilatation

#### Global Theory

The complete specification of elastic properties of earth materials generally requires two compressibility indices, such as Poisson's ratio and aquifer compressibility, however this information is not always available. Love (1941) defined parameters of elasticity that describe displacement of a point on the surface of a spherically symmetrical, homogeneous earth in each of three orthogonal directions in a radial coordinate system. Love noted that stress at the free surface of the earth is 0 and strain in the vertical direction is a simple function of strain in the horizontal directions. Then aquifer dilatation due to earth tides can be approximated as the ratio of the change in earth radius to standard earth radius. He used two of the Love numbers, ( $h$ , and  $l$ ) and the tide generation potential,  $W_2$ , to calculate the change in earth radius. Melchior (1956, p. 24) writes this as:

$$\Delta e = \frac{(2h-6l) W_2 (1-2\nu)}{a g (1-\nu)} \quad (17)$$

where,

$$h = 0.62,$$

$$l = 0.11,$$

$W_2$  is the tide-generation potential for each constituent or group of constituents. See Table 1,

$\nu$  is Poisson's ratio (the ratio of longitudinal strain to areal strain in the plane perpendicular to the applied stress).

Poisson's ratio ranges from -1.0 to 0.5 (commonly 0.2 to 0.4),

Table 1.--Constants used in calculation of tide-generation potential, W2. After Melchior (1983, p. 27)

Tide-generation potential, W2	Celestial constituents of W2	Ratio of tidal wave to maximum lunar tide, D'	Frequency, f (radians per day)	Period, $\omega$ (hours)
M2 group				
Principal lunar wave	M2	0.90812	12.1408	12.4206
N2 group				
Lunar eccentricity wave	N2	0.17387	11.9128	12.6586
Lunar evection wave	v2	0.03303	11.9433	12.6263
S2 group				
Principal solar wave	S2	0.42286	12.5664	12.0000
Luni solar declination	K2	0.11506	12.6008	11.9672
Major solar elliptic wave	T2	0.02479	12.5492	12.0164
Minor solar elliptic wave	R2	-0.00354	12.5836	11.9836
O1, daily lunar wave	O1	0.37689	5.84044	25.8193
K1 group				
daily lunisolar wave	K1	-0.53050	6.30039	23.9345
solar elliptic wave	$\psi$ 1	-0.00423	6.31759	23.8693
solar declinational wave	$\phi$ 1	-0.00756	6.33479	23.8045
solar elliptic wave	$\Pi$ 1	0.01029	6.24878	24.1321
solar principal wave	P1	0.17554	6.26599	24.0659
solar elliptic wave	S1	-0.00423	6.28319	24.0000

$g = 9.80 \text{ m s}^{-2}$ , the acceleration due to gravity, and

$a = 6.37 \times 10^6 \text{ m}$ , the mean radius of the planet earth.

A list of all constants used in this paper is shown in table 2. The values used for  $h$  and  $l$  were tabulated by Melchior (1983, p. 418). Values for  $W_2$  were calculated from equations given by Munk and MacDonald (1960).

There are five principal tidal constituents. These are: the principal lunar wave,  $M_2$ ; the lunar-eccentricity wave,  $N_2$ ; the principal solar wave,  $S_2$ ; the daily lunar wave,  $O_1$ ; and the daily lunisolar wave,  $K_1$ . These waves account for approximately 95 percent of the total tidal potential and are included in all computations of  $W_2$ . These five principal constituents and some other constituents that are so close in frequency to the five principal constituents that they cannot be resolved using fewer than six months of data are shown in Table 1.

Munk and MacDonald (1960) determined the tide-generation potential for semidiurnal waves,  $W_{2s}$ , and for diurnal waves,  $W_{2d}$ , to be

$$W_{2s} = 0.5 Z D' g \sin^2 \theta, \quad (18)$$

$$W_{2d} = Z D' g \sin \theta \cos \theta, \quad (19)$$

where,

$Z = 0.5352 \text{ m}$ , the maximum lunar-tide amplitude. Note that both the lunar and solar values of  $W_2$  are calculated using this value,

$D'$  is the amplitude of the tidal wave relative to the maximum lunar tide (table 1), and

$\theta$  is the colatitude (90 minus the site latitude, in degrees).

The configuration of the principle earth tides are shown in figure 3. The diurnal tides,  $O_1$  and  $K_1$  occur once per day and the semidiurnal tides  $M_2$ ,  $N_2$ , and  $S_2$  occur twice per day.  $K_1$  and  $S_2$  are caused by the sun,  $O_1$  and  $M_2$  are caused by the moon, and  $N_2$  is caused by the interaction of the sun and moon together.

Table 2.--Constants used in this paper.

Constant	Value	Units	Material	Reference
Acceleration due to gravity, $g$	9.80	$m s^{-2}$	Earth	Lindburg, 1982, p. 1-38.
Adiabatic lapse rate, $L$	$6.1 \times 10^{-3}$	$^{\circ}C m^{-1}$	dry air	Considine, 1976, p.218.
Density of water, $\rho$	1000	$kg m^{-3}$	water	Lindburg, 1982, p. 1-38.
Earth radius, $a$	$6.37 \times 10^6$	$m$	Earth	Lindburg, 1982, p. 1-38.
Grain compressibility, $\beta_s$	$1.0 \times 10^{-11}$	$m s^2 kg^{-1}$	calcite	Palciauskas and Domenico, 1989.
	$2.6 \times 10^{-11}$	$m s^2 kg^{-1}$	quartz	
	$1.7 \times 10^{-11}$	$m s^2 kg^{-1}$ or $Pa^{-1}$	plagioclase and pyroxene	
Loading efficiency, $\alpha^*$	0.32	dimensionless	fractured carbonate rock	Calculated from data in Muller and Kibler, 1984.
Love numbers, $h$ $l$	0.62	dimensionless	Earth	Melchior, 1983, p. 418.
	0.11	dimensionless		
Matrix compressibility, $\beta$	$1.4 \times 10^{-11}$	$m s^2 kg^{-1}$	fractured carbonate rock	Muller and Kibler, 1984. Lone Mountain Dolomite and Roberts Mountains Fm.
		or $Pa^{-1}$		
Poisson's ratio, $\nu$	0.30	dimensionless	fractured carbonate rock	Muller and Kibler, 1984. Lone Mountain Dolomite and Roberts Mountains Fm.
Universal gas constant, $R$	$2.868 \times 10^{-1}$	$kg m^2 ^{\circ}C s^{-2}$		Considine, 1976, p. 218.
Water compressibility, $\beta_l$	$5.01 \times 10^{-10}$	$m s^2 kg^{-1}$	$0^{\circ}C$	Rouse, 1950, p. 1011
	$4.78 \times 10^{-10}$	$m s^2 kg^{-1}$	$10^{\circ}C$	
	$4.58 \times 10^{-10}$	$m s^2 kg^{-1}$	$20^{\circ}C$	
	$4.46 \times 10^{-10}$	$m s^2 kg^{-1}$	$30^{\circ}C$	
	$4.41 \times 10^{-10}$	$m s^2 kg^{-1}$ or $Pa^{-1}$	$40^{\circ}C$	

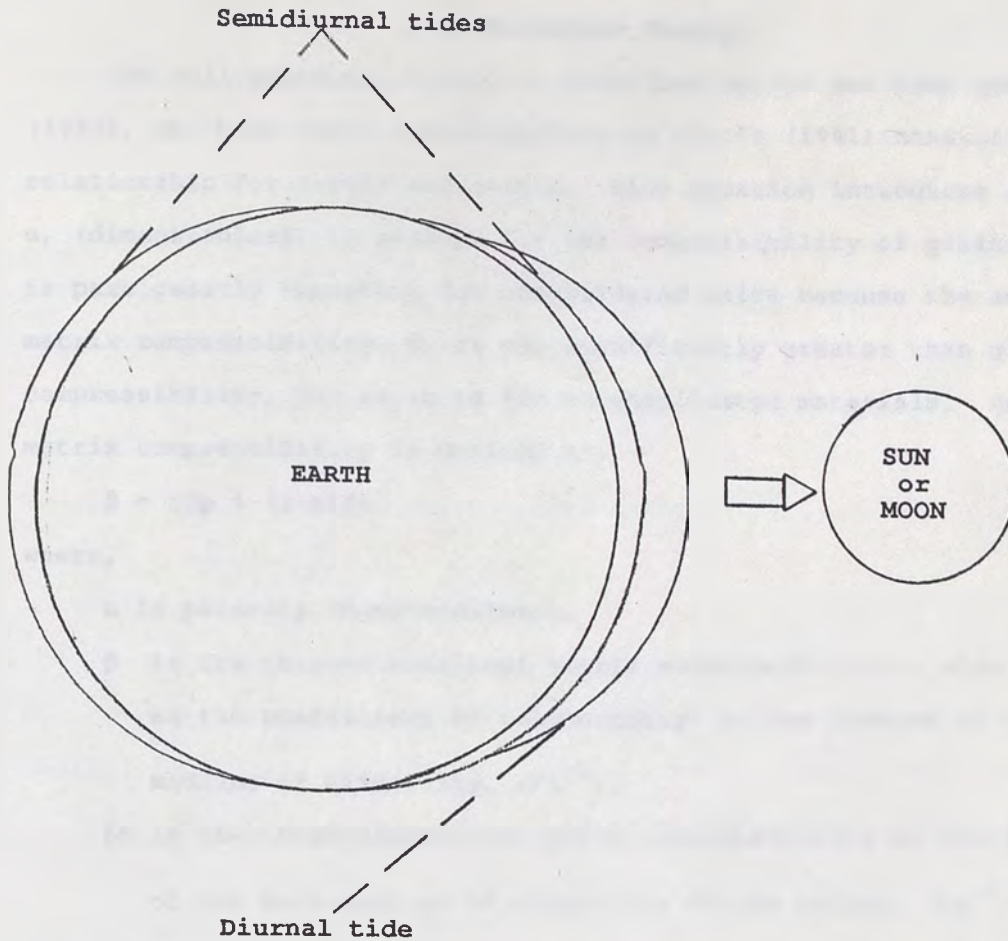


Figure 3.-- Configuration of the diurnal, O1 and K1, and semidiurnal, M2, N2, and S2, earth tides. K1 and S2 are caused by the sun, O1 and M2 are caused by the moon, and N2 is caused by the sun and moon in conjunction.

### Soil Mechanics Theory

The soil mechanics theory is described by Van der Kamp and Gale (1983), who base their investigations on Biot's (1941) constitutive relationship for stress and strain. Biot equation introduces a term,  $\alpha$ , (dimensionless) to account for the compressibility of grains. This is particularly important for consolidated units because the aquifer matrix compressibility,  $\beta$ , is not significantly greater than grain compressibility,  $\beta_s$ , as it is for unconsolidated materials. Aquifer matrix compressibility is defined as:

$$\beta = n\beta_p + (1-n)\beta_s. \quad (20)$$

where,

$n$  is porosity (dimensionless),

$\beta$  is the three-dimensional matrix compressibility-- also known as the coefficient of volume change or the inverse of the bulk modulus of elasticity, ( $\text{Pa}^{-1}$ ),

$\beta_s$  is the three-dimensional grain compressibility or the inverse of the bulk modulus of elasticity of the solids, ( $\text{Pa}^{-1}$ ), and

$\beta_p$  is the three-dimensional pore compressibility ( $\text{Pa}^{-1}$ ).

For an aquifer in which grain compressibility is important, the term  $\alpha$ , a loading efficiency, represents the fraction of rock strain accommodated by collapse of the pores. It may range from near 0 for unfractured consolidated rock, to 1 for unconsolidated rock.

$$\alpha = \frac{\beta - \beta_s}{\beta} \sim \frac{n\beta_p}{\beta} \quad (21)$$

which is more commonly shown as:

$$\alpha = 1 - \beta_s/\beta. \quad (22)$$

Van der Kamp and Gale (1983) define the aquifer dilatation due to earth tides using the rigidity modulus of an aquifer,  $G$ , instead of matrix compressibility, but this term is not well suited to the current study, because it is an additional unknown parameter to be estimated. Instead, the author uses the derivation presented by Van der Kamp and Gale (eqn. 35) prior to introduction of the rigidity modulus term.

$$\Delta e = \rho g dhw'' \beta \frac{1}{TE} - \alpha, \quad (23)$$

which can be written in terms of barometric efficiency as:

$$\Delta e = \rho g dhw'' \beta \frac{1}{1-BE'} - \alpha. \quad (24)$$

#### Specific Storage

Storage coefficient,  $S$ , was originally named by Theis (1935) and defined in terms of aquifer compressibility by Jacob (1940, eq. 11, p.576). Specific storage was later defined by Hantush (1964). Based on the initial definition of storage coefficient, specific storage is defined as the volume of water released from storage,  $dV_w$ , due to a unit head decline,  $dha$ , per unit volume of aquifer,  $V_a$ . If the assumption is made that the volume of water released from storage  $dV_w$  is equal to the change in volume of the aquifer pores,  $dV_p$ , and that the water is free to move within the aquifer, then specific storage,  $S_s$ , can be written as

$$S_s = \frac{-dV_p}{V_a dha}. \quad (25)$$

For granular aquifers the assumption is often made that the compressibility of solids is negligible compared to the compressibility of the pores and that  $dV_p = dV_a$ . Then specific storage may be written in terms of the change in aquifer volume.

$$S_s = \frac{-dV_a}{V_a dha} \quad (26)$$

This equation is very similar to equation (1) describing aquifer dilatation and allows us to write

$$S_s = \Delta a / dha. \quad (27)$$

For a consolidated aquifer the assumption that solid compressibility is negligible cannot be made. In such an aquifer, only the compression occurring within the pores affects water pressure and compression occurring within the grains does not. For this situation, a term that relates  $dV_p$  to  $dV_a$  is derived based on the definition of the compressibility of the solid material and the compressibility of the matrix.

$$\beta_s = \frac{dV_s}{V_s d\sigma'} \quad (28)$$

$$\beta = \frac{dV_a}{V_a d\sigma'} \quad (29)$$

then,

$$\frac{dV_p}{dV_a} = \frac{(dV_a - dV_s)}{dV_a} = 1 - \frac{dV_s}{dV_a}, \quad (30)$$

$$\frac{dV_s}{dV_a} = \frac{\beta_s V_s d\sigma'}{\beta V_a d\sigma'} = \frac{(1-n)\beta_s}{\beta}, \quad (31)$$

where,  $n = V_p/V_a$ ,  $(1-n) = V_s/V_a$ ,

$$\frac{dV_p}{dV_a} = \frac{\beta - (1-n)\beta_s}{\beta} = \alpha^*. \quad (32)$$

where,  $\alpha^*$ , is a loading efficiency similar to  $\alpha$ , and is the proportion of aquifer dilatation that occurs in the pore spaces. Then specific storage for an aquifer in which grain compressibility is important may be determined from aquifer dilatation.

$$S_s = \frac{-dV_a}{V_a} \cdot \frac{dV_p}{dh}, \quad (33)$$

$$S_s = \Delta e \alpha^*. \quad (34)$$

dhw"

Also note that specific storage has not yet been defined in terms of aquifer compressibility, as several forms of this definition exist.

#### Specific Storage in Terms of Aquifer Dilatation

For the one-dimensional global theory, assuming incompressible grains, the result is (Bredehoeft, 1967, eq. 13 and 25, p. 3081):

$$S_s = \frac{-(2h-6l) W_2 (1-2\nu)}{ag (1-\nu) dhw}. \quad (35)$$

Under the assumption of compressible grains, this becomes:

$$S_s = \frac{-\alpha^* (2h-6l) W_2 (1-2\nu)}{ag (1-\nu) dhw}. \quad (36)$$

The three-dimensional soil mechanics result with compressible grains is (Van der Kamp and Gale, 1983):

$$S_s = \rho g \beta \frac{1}{1-BE'} - \alpha. \quad (37)$$

For incompressible grains,  $\alpha = 1$ .

Storage coefficient,  $S$ , then is computed from specific storage and aquifer thickness,  $b$ ,

$$S = S_s b. \quad (38)$$

### Porosity

For confined and partially confined aquifers, porosity,  $n$ , may be computed from the one-dimensional equation for barometric efficiency (Bear 1972, p.211):

$$BE' = \frac{n\beta l}{\beta + n\beta l} \quad (39)$$

where,

$\beta l$  is the compressibility or inverse of the bulk modulus of liquid water. See table 2,

$n$  is the porosity (dimensionless), and

$\beta$  is the aquifer matrix compressibility or inverse of the bulk modulus of elasticity, in  $\text{Pa}^{-1}$ .

An equation for specific storage can also be written in terms of aquifer matrix compressibility (Jacob, 1940):

$$S_s = \rho g (\beta + n\beta l) \quad (40)$$

Combination of equation (36) and (37) yields

$$n = \frac{BE' S_s}{\beta l \rho g} \quad (41)$$

### Aquifer Matrix Compressibility

Aquifer matrix compressibility is an important component of the computations to estimate storage terms. Although an initial value for aquifer matrix compressibility is usually estimated from other sources, a site specific value may be estimated when specific storage and porosity have been calculated. A rearrangement of equation (40) yields

$$\beta = \frac{S_s}{\rho g} - n\beta_1 \quad (42)$$

The method involves an iterative procedure in which a value of aquifer matrix compressibility is assumed and then it is used to calculate  $\alpha^*$ , specific storage, storage coefficient, porosity, and finally aquifer matrix compressibility using equation (42). When the assumed value is within a given error (0.05 seems appropriate) of the value calculated using equation (42), the assumed value is the correct value.

### METHODS OF INVESTIGATION

Harmonic analysis is the decomposition of a periodic disturbance into its principal components by frequency. The technique allows us to determine the amplitudes and phases of perturbations caused by recurring phenomena. The five principal components of the lunisolar perturbation are the driving force of the earth tide, and their frequencies are known to great precision from astronomical observations. The method works best on data sets that contain no gaps, and relatively low levels of high or low frequency noise. For this reason, a complex preparation is required prior to the actual analysis. This section details the steps necessary to prepare for and execute harmonic analysis, and includes discussion of various methods and some common problems. An algorithm specifying the steps involved is shown in figure 4.

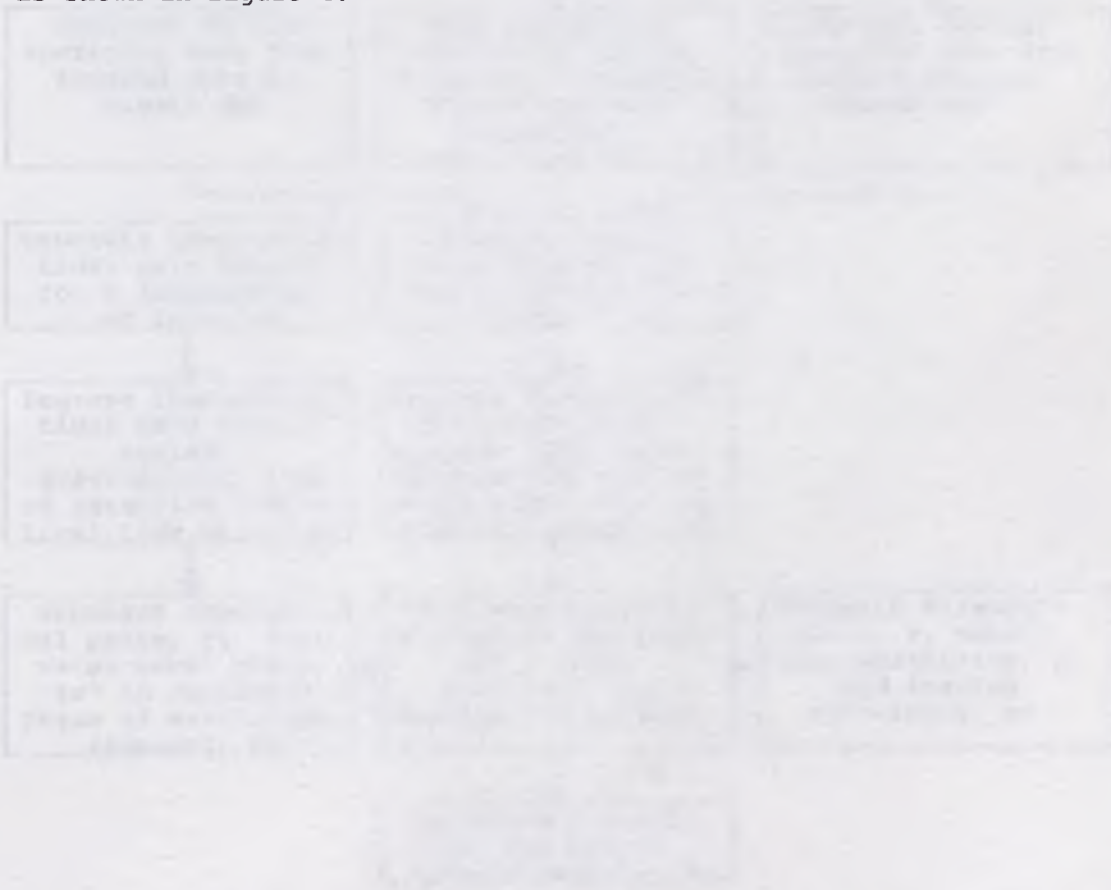


FIGURE 4. ALGORITHM FOR HARMONIC ANALYSIS

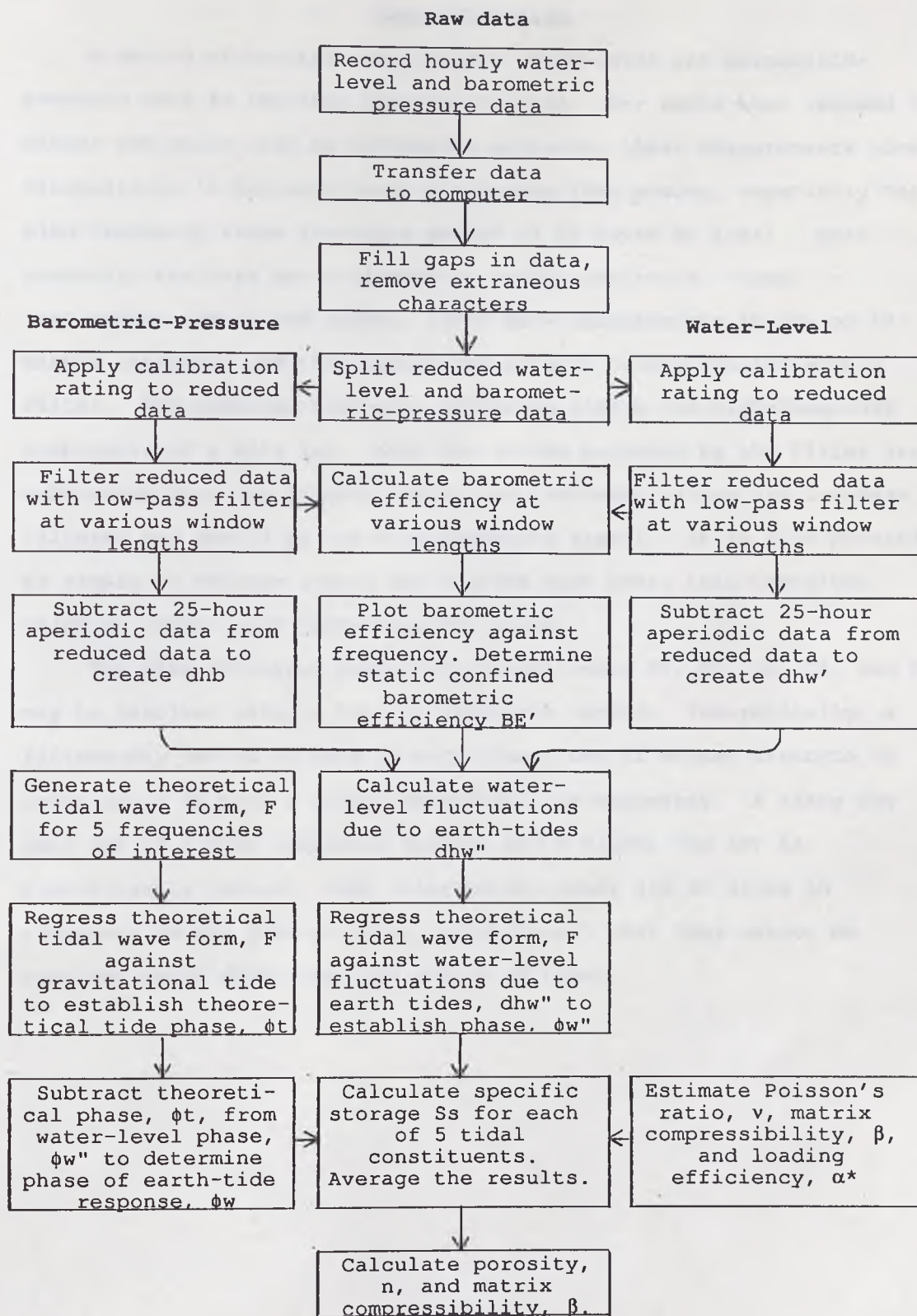


Figure 4.--Harmonic-analysis algorithm.

### Data Collection

A record of uninterrupted hourly water-level and barometric-pressure data is required for the analysis. For wells that respond to either the earth tide or barometric pressure, these measurements show fluctuations in pressure head at numerous frequencies, especially the high-frequency range (having a period of 24 hours or less). Most commonly, the data are collected at hourly intervals. Some researchers (Hsieh and others, 1987) make measurements at 10- or 15-minute intervals and then reduce the data to hourly spacing with a filter. For example, high-pass filtering yields the high-frequency components of a data set. When the values produced by the filter are subtracted from the original data, the remaining values are low-pass filtered and devoid of the high-frequency signal. It is also possible to sample an average over a few seconds each hour; this technique helps to reduce very high-frequency noise.

The five principal earth-tide constituents M2, N2, S2, O1, and K1 may be resolved using a two- to six-month record. Theoretically, a fifteen-day record of data is sufficient, but if signal strength to noise ratio is poor a longer record will be necessary. A sixty day data set is a more realistic minimum and a ninety day set is significantly better. Some other constituents are so close in frequency to the five principal constituents that they cannot be resolved using fewer than six months of data.

The water-level and barometric-pressure-head data should be converted to a consistent set of units. Furthermore, water-level data should be expressed as water level above an arbitrary datum, not as depth below land surface. Ideally, barometric-pressure-head data should be collected at the site. It is permissible however, to use pressure data from local airports. For wells located more than fifty meters above or below the altitude of the airport station, corrections for differences in air density and ambient temperature should be applied. The equation for this is known as the dry-adiabatic pressure relationship (Considine, 1976, p.218):

$$P_s = P_o \frac{[T_o - L dH]^{g/RL}}{[T_o]} \quad (43)$$

where,

$P_s$  is the estimated barometric pressure at the site, in  $\text{kg m}^{-2}$

$P_o$  is the observed barometric pressure at the airport station, in  $\text{kg m}^{-2}$

$T_o$  is the observed temperature at the airport station, in  $^{\circ}\text{K}$ ;

$L = 0.0061 \text{ }^{\circ}\text{C/m}$ , (the dry adiabatic lapse rate, which is the change in temperature of a compressible mass as it undergoes compression or expansion, assuming dry air and no transfer of heat or mass);

$dH$  is the change in altitude from the airport to the well site (positive values indicate an increase in altitude, in m); and

$R = \text{Universal gas constant } (2.868 \times 10^{-1} \text{ kg m}^2 \text{ C}^{\circ} \text{ s}^{-2})$ .

Abrupt discontinuities in the data set are problematic and should be avoided. Both the filtering and harmonic analysis are very sensitive to discontinuities in the original data. The resulting error is known as the Gibbs phenomenon. Discontinuities are easy to correct for, if they are detected, and if a rational explanation for them is available. Long-term trends in water-level measurements, such as drawdown due to nearby pumping wells, stretching transducer cables, and seasonal variations in water level, lead to small errors in barometric efficiency. Graphs of water-level and barometric-pressure data sets should be plotted so that potential problems can be detected early in the analysis. Sometimes a low-pass filter (using an approximately 200-hour window) can be used to remove such trends by subtracting the low-pass trend from the data set.

Some methods of harmonic analysis (such as Fourier transform and regression methods where independent values are created from an equation) cannot accommodate gaps in the data set. There are a number of ways to deal with these gaps. Gaps shorter than twelve hours can most easily be replaced by linear interpolation or cubic-spline interpolation between end points. Longer interruptions, on the order of several days, may be replaced by duplicating data just prior to and just following the gap. Numerous, more elaborate mathematical techniques exist for filling gaps in time-series data. Some cubic- and parametric-spline interpolation methods will satisfactorily fill larger gaps. These methods introduce a small bias that is proportional to the fraction of data which is missing. Data sets produced by the above procedures will henceforth be referred to as reduced records or reduced data.

### **Filtering**

Low-pass filters are applied to the reduced water-level and barometric-pressure-head data in order to distinguish periodic (tidal and solar barometric) from aperiodic (long-term barometric) signals. These components of the signal are separated for two reasons: (1) Few methods of harmonic analysis can accurately handle data with noise that has an amplitude larger than the signal being sought. In this study, the high-frequency noise is usually smaller in amplitude than the signal, so its removal is not critical, but low-frequency noise has a much larger amplitude than the signal and must be removed. (2) The semidiurnal and diurnal signals are produced by both barometric and earth-tide events, which need to be distinguished. Low-frequency events are caused primarily by barometric events such as weather fronts, so the aperiodic signal component can be used to calculate barometric efficiency.

A low-pass filter is used to calculate a moving average from the reduced data. It has a window over which averaging takes place that can be adjusted depending on the frequencies to be filtered. The periodic part of the signal is distinguished by subtracting the aperiodic component (produced by the low-pass filter) from the reduced data according to equation (11). The filter interval or window is closely related to the frequency of the spectrum it filters, a large window filters longer periods.

The periodic part of the data is needed to compute amplitude ( $d_{hw}$ ) and phase angle ( $\phi_w$ ). Extracting the periodic data requires a window that is equal to or just slightly larger than the longest tidal frequency. Shorter windows tend to act partially as high-pass filters. Therefore, a twenty-five-hour window was chosen for this computation, also, because the window's midpoint corresponds to an hourly value, subtraction of the aperiodic function from the reduced data set is a simple matter. An even window length has its midpoint half an hour out of phase with the reduced data set, from which it must be subtracted, thus introducing an undesirable and easily avoided phase error.

Several low-pass filters are available. Perhaps the simplest conceptually is the moving-average filter. By taking the average value over a short interval, only long-term trends are included in the filter values. Subtraction of the filter from the original data yields only the high pass (high frequency) signal. The moving average is computed by

$$A_p(t) = A_n / x. \quad (44)$$

where,

$A_p(t)$  is the aperiodic signal at time  $t$ ,

$A_n$  is the sum 0 to  $x$  of  $h(t)$  (the moving-average operator),

$h(t)$  is pressure head at time  $t$ ,

$x$  is window size, and

$t$  is the time value associated with the filtered value.

T may be further defined as

$$t = t_0 + 0.5(x-1). \quad (45)$$

where,  $t_0$ , is the initial time value in the window. Godin (1972, p. 106) argues that the simple moving average is prone to a problem known as aliasing. The moving-average filter does not remove all of the frequencies close to the window value, and so part of the perturbation that belongs in the filtered data is missing. Godin describes a better low-pass filter:

$$A_p(t) = (A_x A_{(x+1)}^2) / [x(x+1)^2]. \quad (46)$$

where,  $A_{(x+1)}^2$  is the moving average of the moving average at the  $(x+1)$  step. Godin's filter assumes that the time value,  $t$ , is defined as in equation (45). His filter was used in this study.

### Barometric Efficiency

Barometric efficiency, BE, defined in equation (4), (15) and (16), also referred to as gain or one minus the loading efficiency, is an approximation of how much of the barometric pressure is borne by the aquifer grains. A large value for barometric efficiency indicates a rigid (low-compressibility) aquifer that is confined, and a small value indicates either a soft aquifer or partial confinement. Several methods exist for the computation of barometric efficiency. One method that is commonly used in studies of confined aquifers is the scribble plot (Figure 5), in which the aperiodic part of barometric-pressure changes (long-term trends) is plotted against the aperiodic part of water-level fluctuation. The most commonly occurring slope is used to approximate barometric efficiency, because it represents long periods of equilibrium between barometric-head changes and aquifer effects. Short periods of disequilibrium that occur when barometric pressure reaches a culmination and aquifer effects lag behind show up on the graph as sharply curved line segments. The best estimate of barometric efficiency for the plot shown in Figure 5 is 0.31. A modified approach is to compute barometric efficiency according to equation (4) for each one-hour interval of the data set. Excluding the lower and upper 5 percent of the data yields a trimmed-mean value for barometric efficiency of 0.32 (Figure 6).

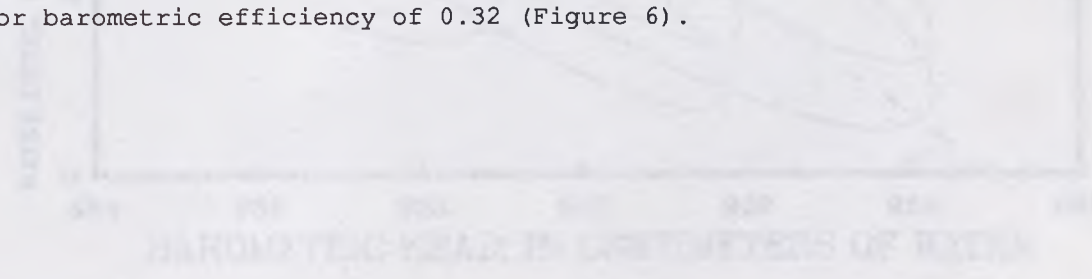


FIGURE 5. — Scribble plot showing the relationship between barometric pressure changes and water-level fluctuations. The plot shows a general upward trend with some local fluctuations and sharp curved segments. The best estimate of barometric efficiency for the plot shown in Figure 5 is 0.31.

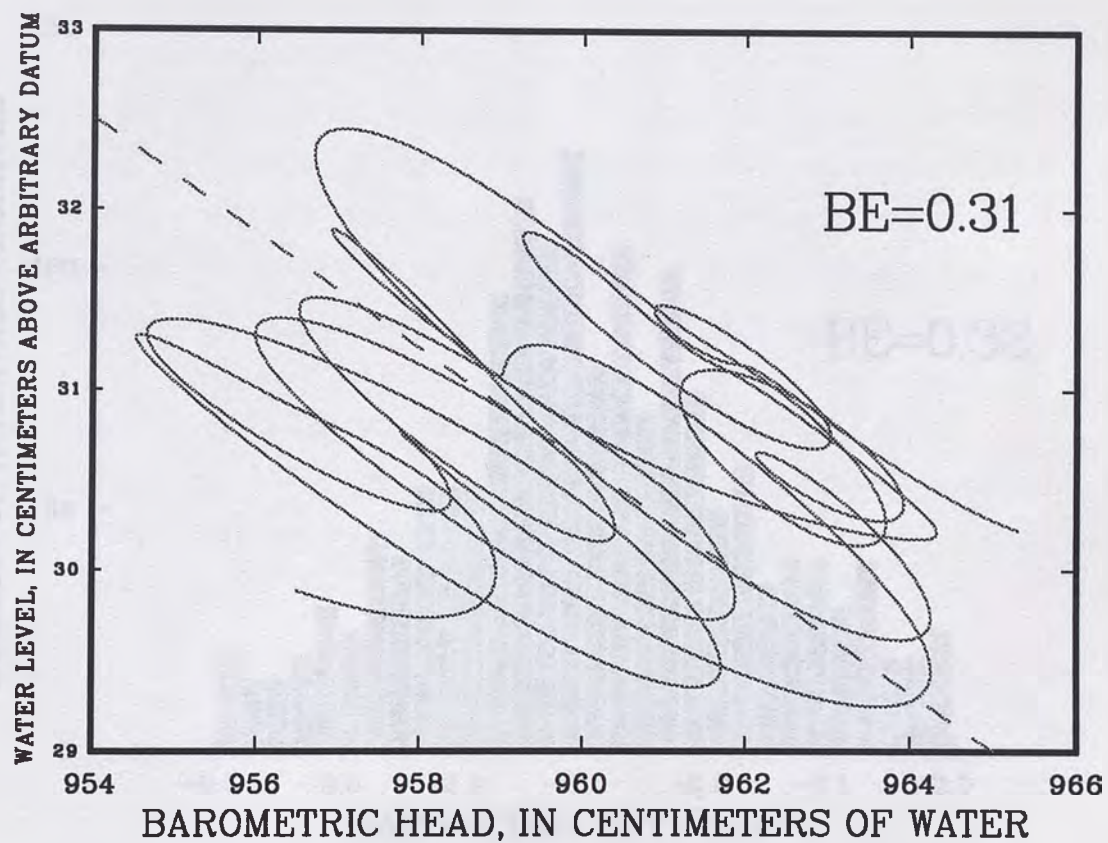


Figure 5.--Aperiodic barometric-pressure head against aperiodic water level at Devils Hole, Nevada. Dashed line shows commonly occurring slope used to estimate barometric efficiency, BE.

Bojarski (1952) and Bojarski and Jones (1957) report that, for partially confined aquifers, barometric efficiency is not constant but is frequency dependent. Bojarski showed that for a well in such an aquifer, plots of barometric efficiency and the frequency at which it is measured have a reciprocal form that can be used to determine the static confined barometric efficiency of a particular data set. Such a curve characteristically has three parts: a low, intermediate, and high frequency, the barometric efficiency is respectively attenuated, amplified, and static confined. See figure 6.

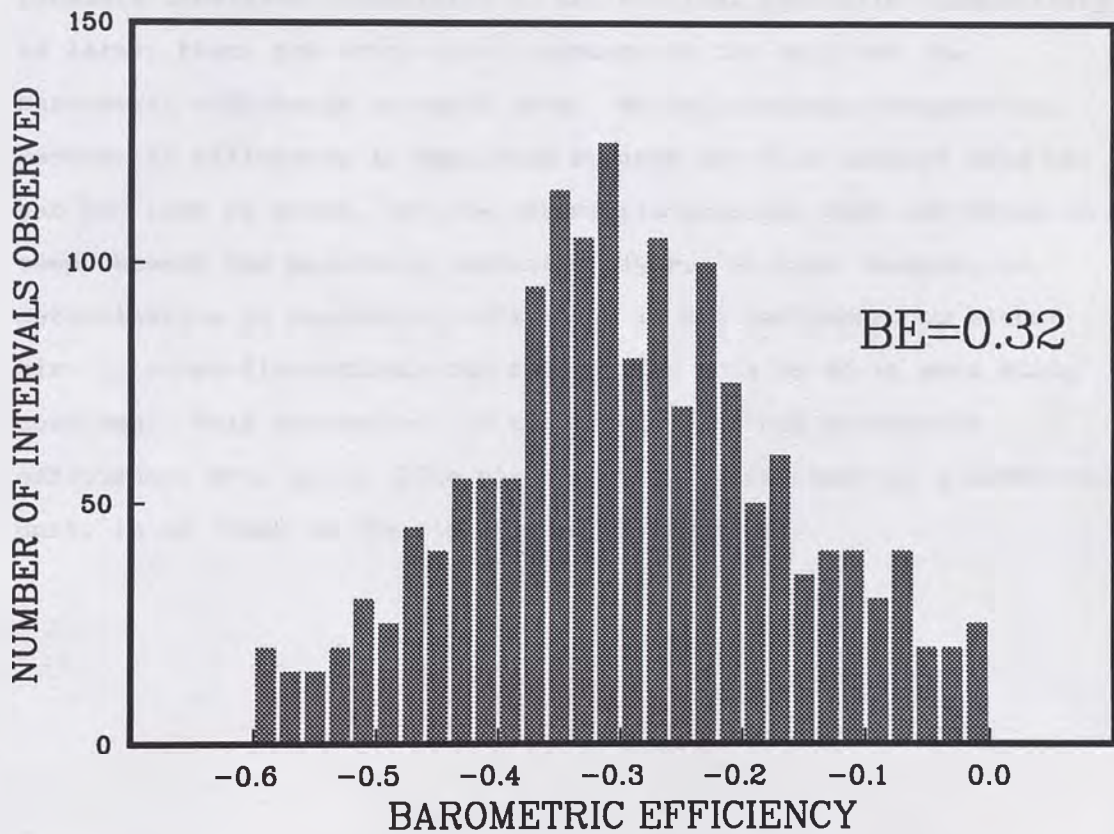


Figure 6.-- Barometric efficiency at Devils Hole, Nevada.

Rojstaczer (1988B) and Rojstaczer and Agnew (1988) report that, for partially confined aquifers, barometric efficiency is not constant but is frequency dependent. Rojstaczer showed that for a well in such an aquifer, plots of barometric efficiency and the frequency at which it is measured have a fundamental form that can be used to determine the static confined barometric efficiency of a particular data set. Such a curve characteristically has three parts: At low, intermediate, and high frequencies, the barometric efficiency is respectively attenuated, amplified, and static confined. See figure 7. At low frequencies, attenuation is caused by equilibration of the pressure imbalance, especially if the vertical hydraulic conductivity is large; then, the water-level response in the well and the barometric efficiency approach zero. At intermediate frequencies, barometric efficiency is amplified because out flow effects have not yet had time to occur, but the barometric-pressure wave has begun to seep through the partially confining layer. At high frequencies, determination of barometric efficiency is not influenced by either air- or water-flow effects and the aquifer acts as if it were fully confined. This corresponds to the static-confined barometric efficiency,  $BE'$ , which, like the barometric efficiency of a confined unit, is an index of the rigidity of the aquifer.

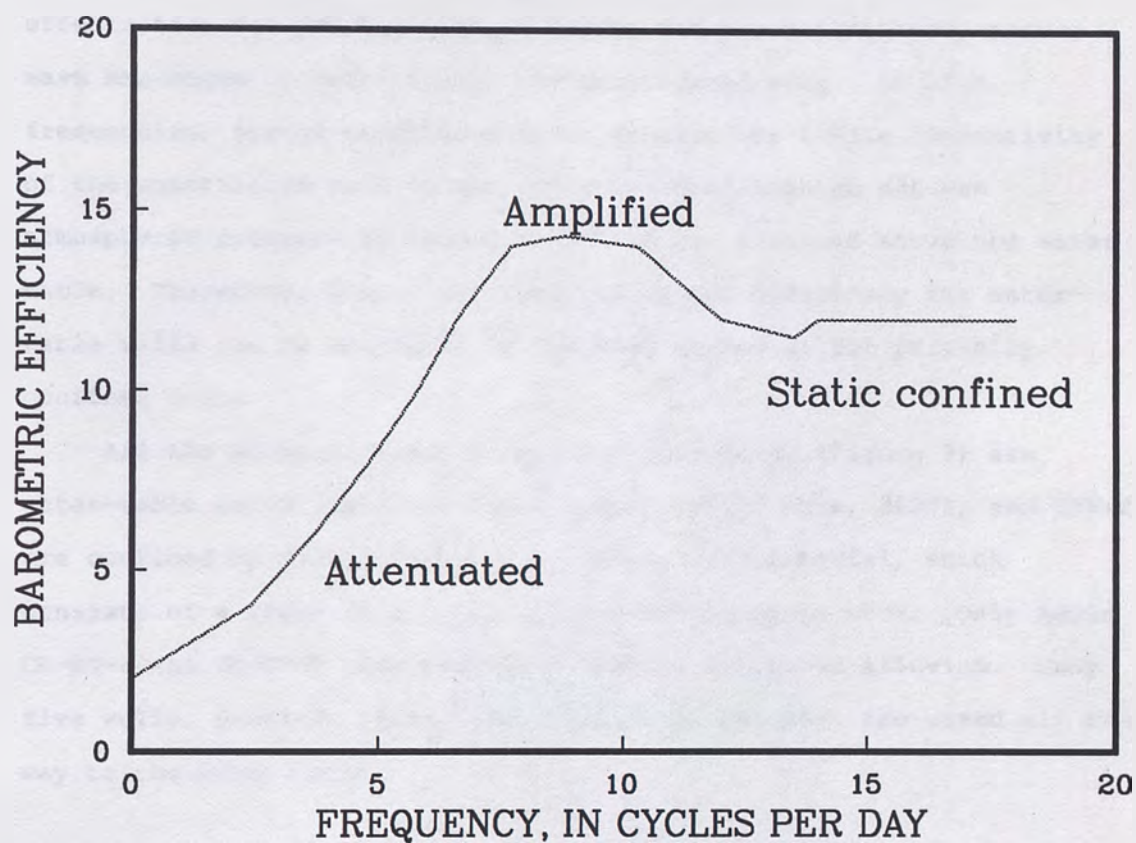


Figure 7.—Relation between barometric efficiency and frequency at which it is calculated for a well in a partially confined aquifer. After Rojstaczer (1988, figs. 3 and 4).

The method of Rojstaczer (1988B) can also be applied to water-table aquifers, if the unsaturated zone is thick enough to act as a partially confining unit and if the well is cased from the surface down to the water table. At low frequencies, attenuation is caused by equilibration of the pressure imbalance, especially if the pneumatic diffusivity (permeability to air) of the unsaturated zone is large. At intermediate frequencies, amplification occurs because out flow effects have not yet had time to occur, but the barometric-pressure wave has begun to seep through the unsaturated zone. At high frequencies, static conditions occur because the finite conductivity of the unsaturated zone to air prevents equilibration between atmospheric pressure at land surface and air pressure above the water table. Therefore, static confined barometric efficiency for water-table wells can be estimated in the same manner as for partially confined units.

All the wells measured as part of this study (Figure 8) are water-table wells. All but three sites, Devils Hole, 36DD1, and CSV-2 are confined by over 100 meters of unsaturated material, which consists of a layer of alluvium overlying carbonate rock. Only wells CE-DT-4 and CE-VF-2 penetrate more than 50 meters of alluvium. Only five wells, SV-DT-2, 36DD1, SBH-2, CE-VF-2, and DR-1 are cased all the way to the water table.

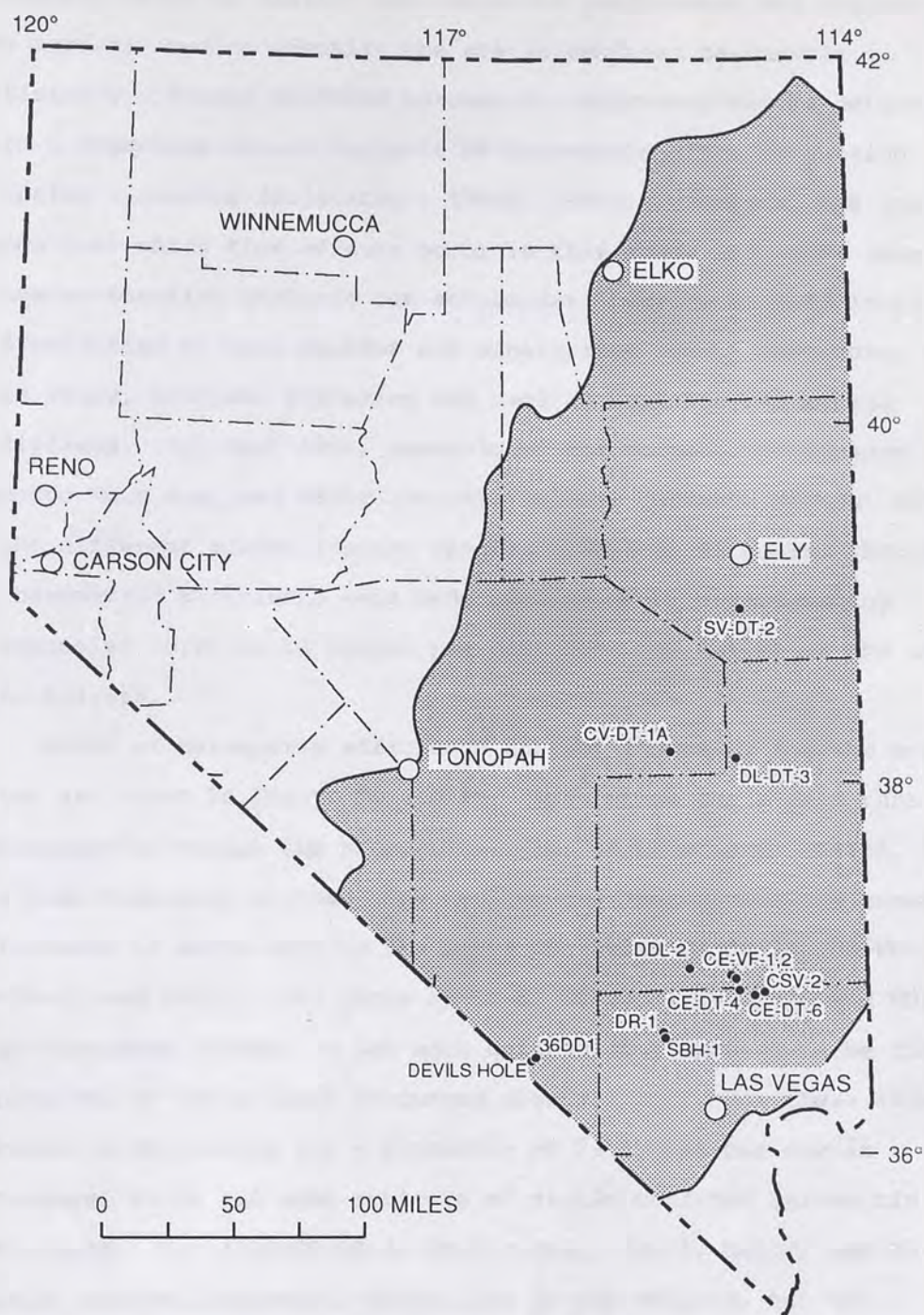


Figure 8.--Location of study sites, shaded area indicates area of carbonate-rock aquifer.

The barometric response of a well-aquifer system with respect to frequency helps to clarify the nature of confinement and rigidity of the aquifer, and to identify the static confined barometric efficiency. Static confined barometric efficiency may be determined from a frequency-domain analysis of barometric efficiency using transfer functions (Rojstaczer, 1988A, 1988B). However, the frequency range over which flow effects occur in this study is higher than transfer-function analysis can accommodate because of very large diffusivities of both aquifer and unsaturated zone. Therefore, for this study, low-pass filtering was used to estimate barometric efficiency. For each site, water-level and barometric-pressure records were analyzed using low-pass filters (Godin's method) with eight different window lengths ranging from 1 to 96 hours. Estimates of barometric efficiency were made for the eight corresponding frequencies (0.25 to 24 cycles per day) from the output of the low-pass filters.

Plots of barometric efficiency against frequency for the study sites are shown in Figure 9a and 9b. Each graph has a form that approximately mimics the theoretical plot of Rojstaczer (1988A, B). The high-frequency plateau that defines the static confined barometric efficiency is shown best by the plots for wells CV-DT-1A, CE-VF-1, CE-VF-2, and CSV-2. For sites DL-DT-3, CE-DT-4, SV-DT-2, and DDL the high-frequency plateau is not well defined, but appears to be closely approached by the highest frequency observations. For these sites the barometric efficiency for a frequency of 24 cycles per day is considered to be the best estimate of static confined barometric efficiency. For sites CE-DT-6, Devils Hole, SBH-1, 36DD1, and DR-1 static confined barometric efficiency is not defined, but was estimated to lie at the break in slope on the low frequency tail of the plots. Barometric efficiencies for frequencies greater than 24 cycles per day is not available because field data were collected at intervals of 1 hour.

The frequency at which the maximum barometric efficiency occurs has been related to pneumatic diffusivity by Rojstaczer (1988B). Wells CE-VF-1, DL-DT-3, CE-VF-2, and CSV-2 have a maximum barometric efficiency at low frequencies (less than 1 cycle per day). Three of these wells penetrate more than 180m of valley-fill alluvium and well CSV-2 penetrates only 5m of alluvium, but is shaley below 90m. The rest of study sites have their maximum barometric efficiency at frequencies of about 4 to 12 cycles per day and penetrate less than 45m of alluvium. No effort was made to calculate pneumatic diffusivity from these data.

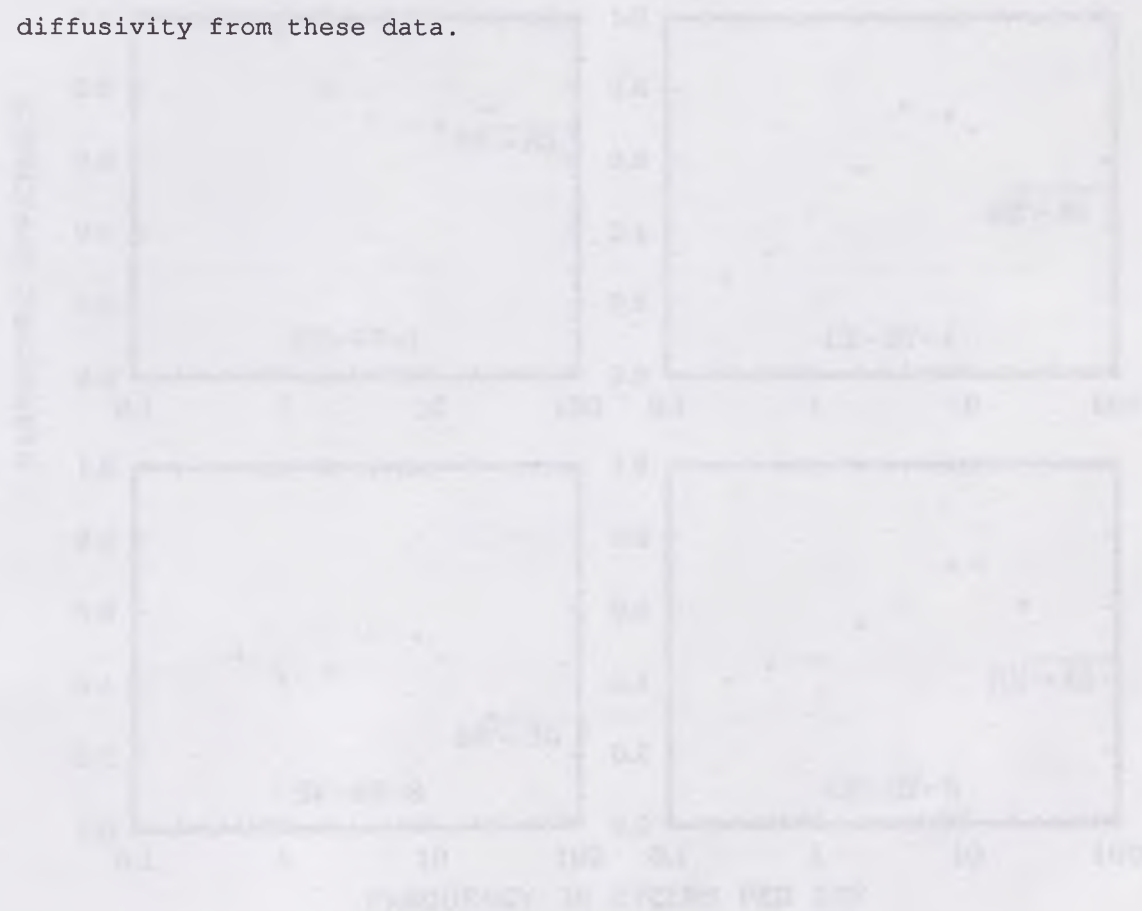


Figure 2. Barometric efficiency vs. frequency of pumping.

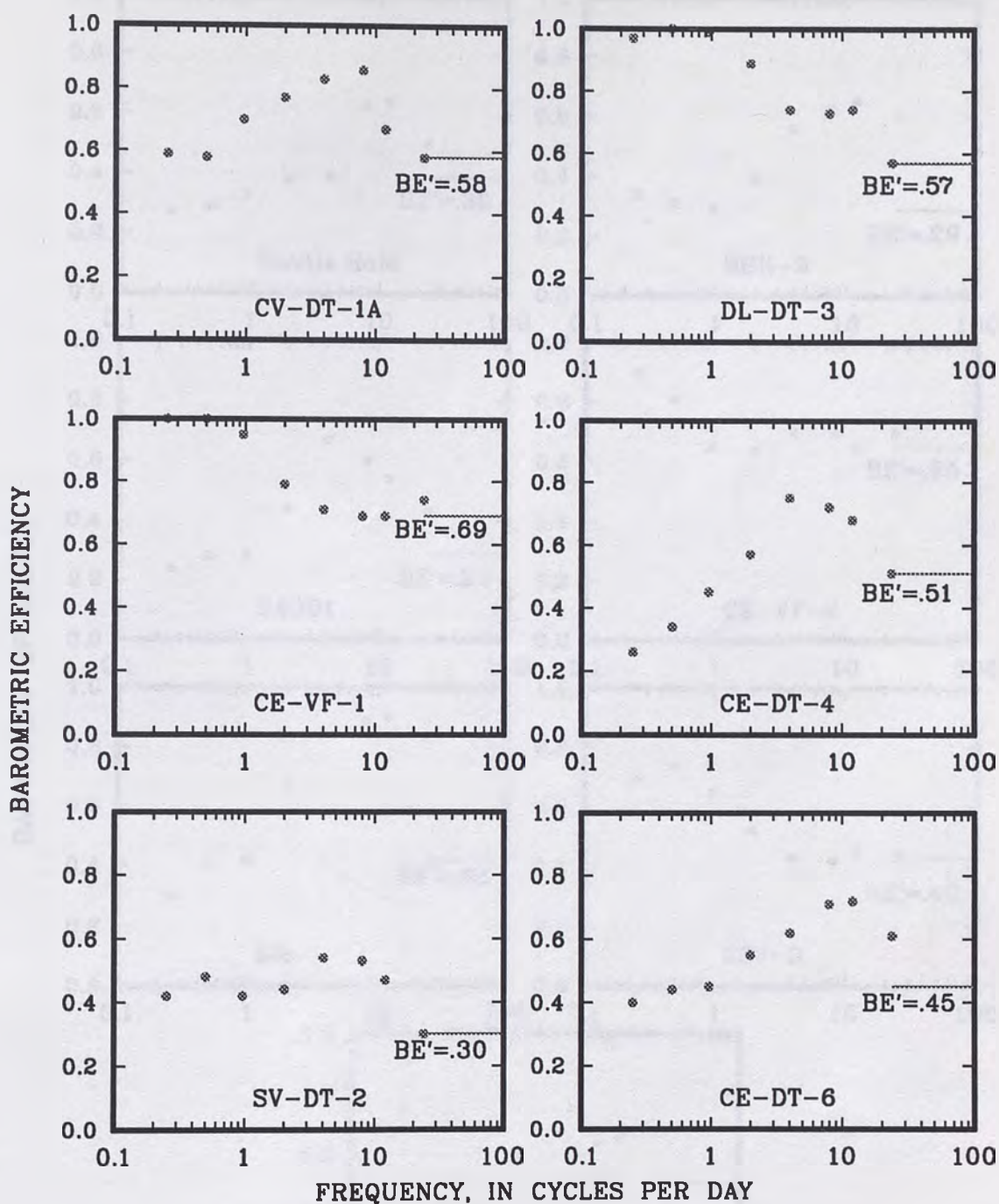


Figure 9a.-- Barometric efficiency as a function of frequency.

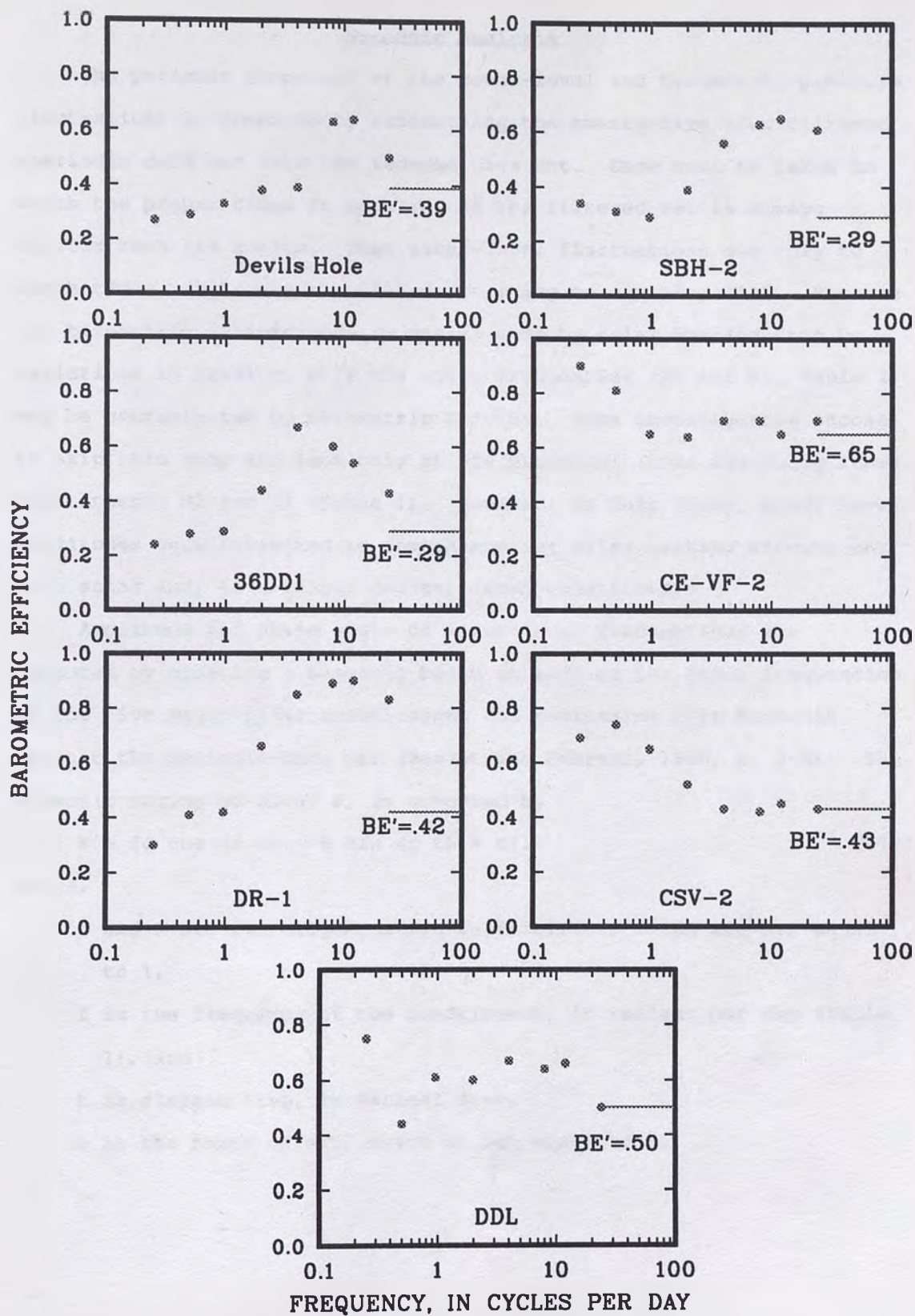


Figure 9b.-- Barometric efficiency as a function of frequency.

### Harmonic Analysis

The periodic component of the water-level and barometric-pressure fluctuations is computed by subtracting the twenty-five hour filtered aperiodic data set from the reduced data set. Care must be taken to match the proper times in each set as the filtered set is always shorter than its source. Then water-level fluctuations due only to earth tides,  $dh_w$ , are calculated according to equation (11). Because the barometric interference is caused more by solar heating than by variations in gravity, only the solar frequencies (S2 and K1, Table 1) may be contaminated by barometric effects. Some investigators choose to skip this step and look only at the principal lunar and daily lunar constituents M2 and O1 (Table 1). However, in this study, water-level amplitudes were corrected to compensate for solar heating effects on both solar and, to a lesser degree, lunar constituents.

Amplitude and phase angle of water-level fluctuations are computed by creating a harmonic based on each of the known frequencies of the five major tidal constituents and regressing this harmonic against the periodic-data set (Bendat and Piersol, 1986, p. 1-9). The harmonic string of data,  $F$ , is computed by

$$F = [J \cos (f t) + K \sin (f t) + b]. \quad (47)$$

where,

J and K are the trigonometric coefficients, which are set equal to 1,

f is the frequency of the constituent, in radians per day (Table 1), and

t is elapsed time, in decimal days,

b is the phase offset, which is set equal to 0.

The regression equation for a given tidal constituent, is of the same form, where,

J and K are the trigonometric coefficients from which amplitude and phase angle may be calculated; and

b is the residual (b~0 if the low-pass moving-average filter has been subtracted from the data set).

Amplitude, A, may be computed from

$$A = (J^2 + K^2)^{1/2}. \quad (48)$$

Phase angle,  $\phi_w''$  may be computed from

$$\phi_w'' = [\arctan (-K/J)] + C \quad (49)$$

where, C=0 if M>0, C=-180° if M<0 and N>0, and C=+180° if M<0 and N<0.

The phase angle must be corrected to the time of the local earth tide.

A program that computes the complex harmonic of the earth tide

(Longman, 1959) is used to generate a data set for the same time

period as the water-level data. The local earth tide is also

regressed against the artificial data set, and the phase angle is

computed. Then tide phase angle,  $\phi_t$  is subtracted from  $\phi_w''$  to yield

the water-level phase,  $\phi_w$ :

$$\phi_w = \phi_w'' - \phi_t. \quad (50)$$

### Instrumentation

Water-level measurements were recorded with both electronic and mechanical instrumentation. Measurements were made at ten sites with pressure transducers equipped with breather cables. The breather cable, or vent tube, allows the transducer to measure gage pressure. If transducers without breather cables are used, barometric pressure must be subtracted from the water-level record to compute the change in head in the well, dhw. Each transducer was installed one to three meters below the water surface. Calibrations were carried out both in the office and in the field so that differences in temperature, altitude, voltage, and cable length could be determined and accounted for. Data were recorded as millivolt signals on either cassette-tape or magnetic-storage modules. Information on well locations, specifications, and instrumentation is presented in table 3.

#### **Pressure Transducers**

Three different types of pressure transducers were used to measure water levels in wells. A vibrating-wire transducer was used in five of the deeper wells. It yields an amperage signal that is converted to millivolts by linking a resistor in parallel with the transducer circuit. This arrangement minimizes signal loss, calibration errors due to long cable length, and, of the three transducers is the least sensitive to temperature fluctuations.

A six-wire full-bridge transducer, which outputs a voltage signal and internally compensates for changes in cable length and voltage, was used in four wells. The six-wire configuration requires a data logger that can handle two separate differential measurements. Unfortunately, this transducer's decreased sensitivity to changes in input voltage is offset by increased temperature sensitivity of the data logger when wired in this configuration.

Table 3.--Well or site location, specifications, and instrumentation

[After Berger and Kilroy (1988, p. 3), Schaefer and others (in press 1990), and Hoffman (1988)].

Well or site designation Used in this study <sup>1</sup>	Local site identification <sup>2</sup>	Location		Land- surface altitude (meters)	Depth			Diameter or di- mensions (meters)	Instru- ment
		Lat(N)	Long(W)		of well	to water	top of screen		
CV-DT-1A	171 N03 E59 10BD1	38°07'58"	115°20'46"	1694.8	559.3	244.1	36.0	0.20	5-psi-amp. transducer
CE-VF-1	210 S12 E63 29DDCC1	36°52'32"	114°55'44"	751.1	217.6	167.1	189.0	0.051	5-psi-amp. transducer
SV-DT-2	171 N12 E63 12AB1	38°55'21"	114°50'36"	2231.1	289.6	125.6	152.4	0.152	Float
DL-DT-3	181 N03 E63 28DA1	38°05'31"	114°53'42"	1658.1	730.0	260.0	236.2	0.20	5-psi-amp. transducer
CE-DT-4	210 S13 E63 23DD1	36°47'43"	114°53'31"	664.5	203.9	107.3	15.2	0.251	5-psi-amp. transducer
CE-DT-6	210 S13 E64 35AA1	36°46'04"	114°47'13"	701.0	285.6	139.3	99.1	0.251	5-psi-amp. transducer
Devils Hole	230 S17 E50 36DCC1	36°25'32"	116°17'27"	740.7	150.0	9.1	0.0	3x15	Float
36DD1	230 S17 E50 36DD1	36°25'29"	116°17'11"	731.5	75.6	14.6	14.6	0.406	Float
DR-1	212 S16 E58 14A	36°33'32"	115°24'40"	1090.9	292.6	248.5	283.0	0.203	5-psi-volt transducer
SBH-1	212 S16 E58 24D1	36°32'12"	115°24'03"	1059.5	219.5	177.1	202.7	0.254	20-psi-volt transducer
CE-VF-2	210 S12 E63 29DABC1	36°52'27"	114°55'44"	751.0	372.2	183.3	262.1	0.254	20-psi-volt
CSV-2	219 S13 E65 28BDAC1	36°46'50"	114°43'20"	666.3	145.7	118.9	145.7	0.229	20-psi-volt
DDL-2	169BS12 E60 10AD1	36°55'02"	115°13'41"	990.6	140.2	65.9	4.0	0.254	20-psi-volt

<sup>1</sup> See figure 6.

<sup>2</sup>In this table, each site is identified by a short station name, the local (Nevada) site-identification system, and by latitude and longitude. Except for this table, only the short well name (for example SBH-1) is used in this report, for convenience. The local site-identification system used in this report is based on an index of hydrographic areas in Nevada (Rush, 1968) and the rectangular subdivision of the public lands referenced to the Mount Diablo base line and meridian. Each site designation consists of four units separated by spaces: The first unit is the hydrographic area number; the second unit is the township, preceded by an N or S to indicate location north or south of the base line; the third unit is the range, preceded by an E to indicate location east of the meridian; the fourth unit consists of the section number and letters designating the quarter section, quarter-quarter section, and so on (A, B, C, and D indicate the northeast, northwest, southwest, and southeast quarters, respectively), followed by a number indicating the sequence in which the site was recorded. For example, site 212 S16 E58 24D1 is in Las Vegas Valley (hydrographic area 212). It is the first site recorded in the SE 1/4 of section 24, Township 16 South, Range 58 East, Mount Diablo base line and meridian.

A three-wire half-bridge transducer, which outputs a voltage signal, was used in one well. The three-wire configuration is not very temperature sensitive, because the data logger must make only one differential measurement, but it is more sensitive to voltage changes than the six-wire configuration.

#### **Floats**

Three sites were measured with floats and mechanical data recorders. For these sites, the depth to water was less than 126 meters (Table 3) and friction between the well and float assembly appeared to be minimal. Data were recorded on punch tape.

#### **Barometric Pressure**

Barometric pressure at sites CE-VF-1 and SBH-2 was measured with a barometric-pressure transducer. To compensate for the instrument's sensitivity to slight breezes, the average of ten measurements taken at one second intervals was recorded on an hourly basis. Calibration against water head was done in the office and calibration with a hand-held digital barometer was done in the field.

For the rest of the sites, station barometric pressures recorded at Las Vegas McCarran airport and Ely airport were used in the calculations. The data were purchased from the National Climatic Data Center (Asheville, North Carolina), which is operated by the National Oceanic and Atmospheric Administration. The weather data are now available in digital format.

There are several errors associated with the use of off-site barometric data. A phase error of approximately  $3^\circ$  (for all frequencies) is induced because the airports record barometric pressure at approximately 10 minutes before the hour, but water-level measurements were taken on the hour. The usefulness of airport data also decreases with increasing distance from the well site. Wells CV-DT-1A and DL-DT-3 are located approximately 150 kilometers away from Ely airport. All other study sites were located within 100 kilometers of an airport.

Care was taken to shield the barometers and data loggers from fluctuating temperatures. This involved placing the instruments in an ice chest set in the ground so that its top was about 0.1 meter below land surface. A breather cable was installed between the cooler and the atmosphere. Panel temperatures on the data recorder fluctuated no more than 15°C during the period of study despite air temperature fluctuations of approximately 70°C, except during monthly data retrieval, when the ice chest was open to the atmosphere.

#### AQUIFER STORAGE CHARACTERISTICS

Eleven wells and one open fracture that penetrate Paleozoic carbonate units and one well that penetrates only valley-fill alluvium in southeastern Nevada were studied. The locations of these sites, all within a few hundred meters of carbonate-rock outcrops, are shown in Figure 6, and geologic characteristics are listed in Table 4. Except for CE-VF-1, the wells are fully cased in basin-fill material and are open through most of the carbonate-rock section. Only the open fracture, Devils Hole, is located completely in carbonate rock, although alluvium occurs nearby. Each site shows evidence of semidiurnal or less frequent water-level fluctuations, characterized by amplitudes of several centimeters.

Table 4.--Geologic characteristics of study sites

[---not applicable or unknown]

Site	Depth to water (meters)	Depth at bottom of unit (meters)	Principal geologic unit	Geologic Age	Formation
CV-DT-1A	244.1	31.4	Alluvium	Quaternary	---
		138.7	Shale, siltstone	Mississippian	Chainman Shale
		213.4	Limestone	Mississippian	unnamed limestone
		559.3	Dolomite	Devonian	Guilmette Formation
CE-VF-1	167.1	217.6	Alluvium	Quaternary	---
SV-DT-2	125.6	0.7	Alluvium	Quaternary	---
		289.6	cherty limestone	Pennsylvanian	Ely Limestone
DL-DT-3	260.0	59.4	Alluvium	Quaternary	---
		125.0	Tuff	Tertiary	---
		664.5	Dolomite	Devonian	Guilmette Formation
		730.0	Silty limestone	Devonian	Simonsen Dolomite
CE-DT-4	107.3	9.1	Alluvium	Quaternary	---
		203.9	Limestone, chert	Mississippian	Anchor Limestone (Monte Cristo Limestone)
CE-DT-6	139.3	23.8	Alluvium	Quaternary	---
		61.0	Siliceous limestone	Mississippian	Monte Cristo Limestone
		87.2	Sandstone	Mississippian	---
		285.6	Limestone	Mississippian	Monte Cristo Limestone
Devils Hole	9.1	150.0	Limestone, dolomite	Cambrian	Bonanza King Formation
36DD1	14.6	1.8	Alluvium	Quaternary	---
		30.5	Travertine	Quaternary	---
		75.6	Limestone, dolomite	Cambrian	Bonanza King Formation
DR-1	248.5	39.6	Alluvium	Quaternary	---
		42.1	Lacustrine silt, clay	Tertiary	---
		171.6	Limestone	Devonian	Sultan Limestone
		191.1	Shale, dolomite	Silurian	Lone Mountain Dolomite
		292.6	Dolomite	Silurian	Lone Mountain Dolomite
SBH-1	177.1	18.3	Alluvium	Quaternary	---
		61.0	Limestone, dolomite	Ordovician	Antelope Valley Limestone
		122.0	Limestone, dolomite	Ordovician	Ninemile Formation
		219.5	Dolomite	Ordovician	(Pogonip Group)
CE-VF-2	183.8	259.1	Alluvium	Quaternary	---
		304.8	Dolomite	Devonian	Sultan Limestone
		353.6	Limy shale	Devonian	Sultan Limestone
		372.2	Dolomitic limestone	Devonian	Sultan Limestone
CSV-2	118.9	5.2	Alluvium	Quaternary	---
		23.8	Dolomite	Permian	Bird Spring Group
		32.0	Limestone	Permian	Bird Spring Group
		88.4	Silty limestone	Permian	Bird Spring Group
		145.7	Shaley limestone	Permian	Bird Spring Group
DDL-2	65.9	1.8	Alluvium	Quaternary	---
		140.2	Limestone	Ordovician	Pogonip Group

### Estimated Parameters

Several parameters must be estimated prior to computation of storage terms. The Love numbers are used in the calculation of areal dilatation (equation 12). The Love numbers are assumed to be constant at the Earth's surface (Melchior, 1983); regional or more site-specific values are not available at this time.

Poisson's ratio, like hydraulic conductivity, is a second-rank tensor. Although it may have the properties of anisotropy and heterogeneity, it is accepted practice to assume that Poisson's ratio is a constant for a given rock type. A measurement of Poisson's ratio was not available for any of the study wells; however, Muller and Kibler's (1984) values of dynamic Poisson's ratio (derived from the ratio of acoustic velocities) for a nearby well penetrating Silurian carbonates (Lone Mountain Dolomite and Roberts Mountains Formation, chiefly silty limestone) near Yucca Mountain ranged from 0.26 to 0.34. The median value in this range, 0.30 was used in this study as Poisson's ratio for carbonate rocks.

The loading efficiency,  $\alpha^*$ , may have a value ranging from near 0 to 1. This factor may be estimated from measurements of grain and matrix compressibility. Matrix compressibility is not known for any of the study sites, but Muller and Kibler (1984) report a bulk modulus of  $7.0 \times 10^{10} \text{ m s}^2 \text{ kg}^{-1}$  under fully saturated (undrained) conditions. The inverse value ( $1.4 \times 10^{-11} \text{ kg m}^{-1} \text{ s}^{-2}$ ) is the three-dimensional matrix compressibility,  $\beta$ , which, when used in equation (21) with a calcite grain compressibility,  $\beta_s$ , of  $1.0 \times 10^{-11} \text{ kg m}^{-1} \text{ s}^{-2}$  yields an  $\alpha^*$  value of 0.32. This  $\alpha^*$  value is consistent with the range of values 0.20 to 0.44 reported by Van der Kamp and Gale (1983) for fractured granite or marble aquifers.

If the Love numbers,  $h=0.62$ , and  $l=0.11$ , Poisson's ratio  $\nu=0.30$ , earth radius,  $a=6.37 \times 10^6$  m, density of water,  $\rho=1000 \text{ kg m}^{-3}$ , and acceleration due to gravity,  $g=9.80 \text{ m s}^{-2}$  are used, the global equation becomes:

$$S_s = \frac{0.33 \alpha^* W_2}{6.24 \times 10^7 \text{ dhw}''}. \quad (51)$$

The soil mechanics equation becomes

$$S_s = 1.372 \times 10^{-7} \frac{1}{1-BE} - \alpha. \quad (52)$$

#### **Measured Parameters**

Godin's (1972) low-pass filter with a variable window (2, 3, 6, 12, 25, 48, and 96-hours) was used to filter the data set for the calculation of barometric efficiency. Barometric efficiency, as plotted in figure 9a and 9b, is the mean of barometric-efficiency values for each hour of the data set. Static confined barometric efficiencies derived from the graphs range from 0.29 to 0.69 (table 5).

Water-level fluctuations caused by the earth tide,  $\text{dhw}''$ , corrected for barometric effects (using a 25-hour filter and barometric efficiency), vary between 0.1 and 17 millimeter. The rated detection limits of the pressure transducers and barometers are infinite, but the data loggers that record the information limit resolution to about 1.5 millimeters. Float-type measurements have a resolution of around 3 millimeters.



Phase angles,  $\phi_w''$ , calculated using the 25-hour low-pass filter, are shown only for those tidal constituents that exceeded the detection limit. Phase angle is also a function of frequency and may be a function of fracture orientation as well. Average phase-angle for 5 sites (Table 5) are within  $\pm 20^\circ$  of the theoretical norm of  $180^\circ$ . Those sites that do not conform either had less than 3 months' data available (CE-DT-4, DR-1, and SBH-2) or had a very small amplitude response to earth tides (CE-VF-1 and DL-DT-3). Because phase angles appear to be a strong function of data length, no correction was made for phase angles.

Values for the earth-tide dilatation,  $\Delta e$ , were computed from equations (17) and (24) and constants presented in Table 2; they were calculated individually for each one-degree increment of colatitude represented by the sample population (Table 5).

#### Calculated Parameters

Tables 5 and 6 show estimates of specific storage, storage coefficient, porosity, and computed matrix compressibility based on the initial assumption that  $\alpha^* = 0.32$ . The values of computed matrix compressibility are 1 to 4 times larger than the initially assumed value and suggest that the initial value is somewhat too large in most cases. For each site, the initially assumed value of matrix compressibility was lowered until the value computed using equation (40) matched within 0.05 percent.

Table 6.-- Estimated porosity and matrix compressibility based on an assumption of  $\alpha^* = .32$ [± values represent one standard deviation of the mean; for average porosity  $x \leq 5$  (number of Earth-tide constituents used).]

Site	Aquifer thickness (meters)	Storage coefficient, S ( $\times 10^{-5}$ )			Static confined barometric efficiency BE'	Porosity (percent)			Computed matrix compressibility $\times 10^{-11} \text{ Pa}^{-1}$
		incom-pressible	global compressible	soil mechanics		incom-pressible	global compressible	soil mechanics	
CV-DT-1A	315	52.92	16.95	8.91	.58	21.7	7.7	3.7	1.91
CE-VF-1	51	9.84	---	5.92	.69	29.6	---	17.8	6.14
SV-DT-2	164	13.63	4.36	2.49	.30	5.5	2.0	1.0	1.80
DL-DT-3	470	76.61	24.53	12.93	.57	20.7	6.9	3.5	2.17
CE-DT-4	97	11.16	3.57	2.26	.51	13.1	4.2	2.6	1.83
CE-DT-6	146	12.56	4.02	3.01	.45	8.6	3.9	2.1	1.02
Devils Hole	>143	6.00	1.92	2.59	.39	3.6	1.2	1.6	1.90
36DD1	61	7.44	2.37	0.91	.29	7.9	3.6	1.2	2.32
DR-1	44	8.73	2.79	0.85	.42	18.5	4.1	1.8	4.59
SBH-1	42	7.64	2.44	0.63	.29	11.7	7.9	1.0	2.32
CE-VF-2	110			3.83	.65			5.0	4.96
CSV-2	268			5.28	.43			1.9	3.18
DDL-2	74			1.71	.50			2.6	2.00

### Matrix Compressibility

Matrix compressibility occurs in most of the calculations for storage terms and was initially estimated to be  $1.4 \times 10^{-11} \text{Pa}^{-1}$ . Recalculation of matrix compressibility by an iterative process yielded values ranging from  $1.05 \times 10^{-11}$  to  $1.35 \times 10^{-11} \text{Pa}^{-1}$  with an average value of  $1.15 \times 10^{-11} \pm 9 \times 10^{-13} \text{Pa}^{-1}$ . Matrix compressibility for one well in alluvium was  $5.3 \times 10^{-11}$ . See table 7.

Values of loading efficiency,  $\alpha^*$ , derived from these new estimates of matrix compressibility ranged from .06 to .28 with an average of  $.15 \pm .06$ , which is slightly smaller than Van der Kamp and Gale's (1983)  $\alpha$  estimate for Tennessee marble of .20. For alluvium,  $\alpha^*$  is .86.

### Specific Storage

Specific storage for fractured rocks, is commonly in the range of  $1 \times 10^{-6}$  to  $1 \times 10^{-4} \text{m}^{-1}$  and for unfractured rock may reach  $1 \times 10^{-7}$  (Freeze and Cherry, 1979). The global theory with compressible-grains yields estimates of specific storage ranging from  $1.50 \times 10^{-7}$  to  $2.57 \times 10^{-7} \text{m}^{-1}$ , and averaging  $2.09 \times 10^{-7} \pm 4.0 \times 10^{-8}$  the soil mechanics approach with compressible grains yields estimates from  $1.74 \times 10^{-7}$  to  $2.94 \times 10^{-7} \text{m}^{-1}$ . The incompressible grains value of  $1.93 \times 10^{-6} \text{m}^{-1}$  is considered the best estimate of specific storage for the one well in alluvium.

Table 7.-- Revised storage characteristics based on new estimates of matrix compressibility showing porosity estimates from borehole geophysical studies for comparison

Site	Estimated matrix compressibility ( $\times 10^{-11} \text{Pa}^{-1}$ )	Loading efficiency $\alpha^*$	Specific storage, $S_s$ ( $\times 10^{-7} \text{m}^{-1}$ )	Storage coefficient, $S$ ( $\times 10^{-5}$ )	Porosity $n$	Computed matrix compressibility $\times 10^{-11} \text{Pa}^{-1}$	Porosity	
							acoustic density	neutron density
<b>Global Theory, Compressible Grains</b>								
CV-DT-1A	1.14	.15	2.55	8.03	3.3	1.09		
CE-VF-1	5.30	.86	16.6	5.92	25.5	5.25		
SV-DT-2	1.26	.22	1.79	2.94	1.2	1.28		
DL-DT-3	1.14	.16	2.57	12.08	3.3	1.12		
CE-DT-4	1.22	.20	2.34	2.27	2.7	1.17	10.0± 3.9	7.6± 3.0
CE-DT-6	1.35	.28	2.37	3.46	1.3	1.33		2.3± 1.3
Devils Hole	2.00	.51	2.13	3.05	1.8	1.32		
36DD1	1.14	.13	1.62	0.99	1.0	1.17		
DR-1	1.09	.10	1.93	0.85	1.8	1.14		
SBH-1	1.08	.08	1.50	0.63	1.0	1.08		
<b>Soil Mechanics Theory, Compressible Grains</b>								
CE-VF-2	1.15	.13	3.07	3.38	4.4	---	0.7± 1.0	0.7± 1.1
CSV-2	1.15	.13	1.83	4.91	1.8	---	4.2± 1.9	5.0± 2.0
DDL-2	1.15	.13	2.10	1.56	2.3	---		

Both methods yield estimates of specific storage that are an order of magnitude smaller than expected, but reasonable for unfractured media. Although slightly smaller than anticipated, these values, when used in equation (34) yield reasonable estimates of porosity. Few other estimates of specific storage are available for the carbonate aquifers of southeastern Nevada. Well CE-DT-4 has an estimated storativity of 14 percent (J.H. Kleinfelder and others, written communication, 1980), which, when divided by a well screen length of 96 meters yields a specific storage of  $1.5 \times 10^{-3} \text{ m}^{-1}$ . However, because the pump was not able to draw down the highly transmissive aquifer very much at the observation well, this value might be too large.

Galloway and Rojstaczer (1990) used the compressible grain soil-mechanics theory to estimate specific storage of the Lone Mountain Dolomite and Roberts Mountain Formation in the same well that Muller and Kibler (1984) studied (UE-25P#1) underlying volcanic tuff units at the Nevada Test Site. Their study was conducted at a depth of 1805 meters and yielded a specific storage estimate of  $3.46 \times 10^{-9} \text{ m}^{-1}$ . This value is small for either fractured or unfractured material and two orders of magnitude smaller than any of the above estimates. The great depth at which their study was conducted may have influenced their results, which are not realistically comparable to those presented in this paper.

### Storage Coefficient

Storage coefficient is commonly in the range of  $5 \times 10^{-3}$  to  $5 \times 10^{-5}$  (Freeze and Cherry, 1979, p. 60). The global theory estimates of storage coefficient range from  $0.63 \times 10^{-5}$  to  $12.08 \times 10^{-5}$ . The soil mechanics approach yields estimates from  $1.51 \times 10^{-5}$  to  $4.66 \times 10^{-5}$ . The best estimate of storage coefficient for one well in alluvium is  $9.84 \times 10^{-5} \text{ m}^{-1}$ .

The estimates of storage coefficient are mostly within the range suggested by Freeze and Cherry (1979) and are considered reasonable.

### Porosity-Global Theory

The global theory (compressible grains) yields porosity estimates for the carbonate-rock aquifers from 1.0 to 3.3 percent. Three types of outside information constrain porosity estimated in this study. 1) Total porosity determined from borehole geophysical logs of neutron-density (D.L. Berger, written communication, 1989) are available for four wells (CE-DT-4, CE-DT-6, CE-VF-2, and CSV-2) and secondary porosity by acoustic velocity is available for three of the same wells. The measurements range from 0.7 to 10 percent (Berger, 1989). 2) Porosity values for carbonate aquifers at nearby sites are: .06 percent (Galloway and Rojstaczer, 1989); and 4.0 to 6.0 percent (Muller and Kibler, 1984). 3) Transmissivity was determined from specific-capacity tests at seven sites. Use of the transmissivity data is based on the premise that the fractures, which transmit water, are the major components of effective porosity, and therefore porosity and transmissivity are correlated to some extent.

The three largest values of porosity for the carbonate aquifers (2.7 to 3.3 percent) were from well sites where large values were expected (CV-DT-1A, DL-DT-3, and CE-DT-4). Wells CV-DT-1A (3.3 percent) and DL-DT-3 (3.3 percent) penetrate the Devonian Guilmette Formation, which consists principally of cavernous dolomite with abundant joints and bedding-plane fractures. Transmissivities that were derived from specific-capacity tests of wells CV-DT-1A and DL-DT-3 are  $4.3 \times 10^{-4}$  and  $1.4 \times 10^{-2} \text{ m}^2 \text{ s}^{-1}$ . Although the porosity for site CV-DT-1A is somewhat large given the transmissivity, the estimate seems reasonable based on the lithology. Well CE-DT-4 (2.7 percent) penetrates Mississippian Monte Cristo Limestone and correlative cherty limestone. The high transmissivity ( $4.3 \times 10^{-2}$  to  $2.2 \times 10^{-1} \text{ m}^2 \text{ s}^{-1}$ ) due to fracture permeability suggests that the porosity estimate is reasonable, however the neutron-density porosity ( $10.0 \pm 4.2$  percent), acoustic-density porosity ( $7.6 \pm 3.0$  percent) are significantly larger.

Moderate values of porosity (1.8 percent) were encountered at two sites (Devils Hole, and DR-1). Devils Hole yielded a porosity ( $1.8 \pm 0.3$  percent) that was smaller than expected. The site is an open fault in Cambrian Bonanza King Formation limestone and dolomite and is locally unconfined by alluvium. Transmissivity and porosity estimated by other methods are unavailable; however, the size of Devils Hole (approximately 3 m wide by 15 m long and at least 150 m deep), its location along a rather prominent vertical fault, and proximity to regional springs at Ash Meadows suggest a porosity larger than the measured value. Both water-level and barometric-pressure data are considered to be accurate and precise. The cavern wall at Devils Hole is coated with as much as one meter of calcium-carbonate cement that may effectively seal off most other fractures and joints from the main opening. Yet this still does not adequately explain the small estimated porosity. Because the fault has great width, and

lateral continuity, local aquifer dilatations may indeed occur entirely within the cavern itself, without significant compression of carbonate grains. For this reason, the incompressible-grain porosity estimate of 3.6 percent is considered to be the best estimate of porosity at Devils Hole.

Well DR-1, which yielded a porosity of 1.8 percent, penetrates Devonian Sultan Limestone and Silurian Lone Mountain Dolomite. There are no transmissivity data available for this well, and the well is cased to the water table. The calculated value of porosity seems consistent with local lithology and structure.

Four sites (SV-DT-2, CE-DT-6, 36DD-1, and SBH-1) yielded small values of porosity (1.0 to 1.3 percent). Well SV-DT-2 penetrates cherty limestone and shale of the Permian Ely Limestone. The moderate transmissivity,  $2.2 \times 10^{-4} \text{ m}^2 \text{ s}^{-1}$ , suggests that the small porosity value is reasonable. Site CE-DT-6 (1.3 percent) is located approximately 10 kilometers east of well CE-DT-4. Estimated porosity at this site is in pretty good agreement with the neutron-density estimate of  $2.3 \pm 1.3$  percent, however the transmissivity at this site,  $1.4 \times 10^{-1} \text{ m}^2 \text{ s}^{-1}$  is very high. Well 36DD1 (1.0 percent) penetrates limestone and dolomite of the Cambrian Bonanza King Formation and lies about 200 meters east of Devils Hole. No other data are available with which to compare this estimate. Well SBH-1 (1.0 percent), penetrates Ordovician limestone and dolomite (Ninemile Formation of the Pogonip Group), which bear moderately abundant fractures and bedding-plane joints. These rocks have a large transmissivity of  $4.0 \times 10^{-1} \text{ m}^2 \text{ s}^{-1}$ .

The incompressible grains analysis of well CE-VF-1 in alluvium yields a porosity estimate of 25.5 percent, that seems appropriate.

#### Porosity-Soil Mechanics

Water-level fluctuations due to earth tides at three sites (CE-VF-2, CSV-2, and DDL-2) were not large enough to exceed the instrument detection limits, so a response to the earth tide was not estimated.

Only the barometric efficiency was calculated and only the soil mechanics approach was used to calculate storage characteristics. This method is considered to be less precise than the global method because less information is input to the equation. Two of the wells (CSV-2, and DDL-2) are located very close to carbonate-rock outcrops that may cause the carbonate-rock aquifer to behave locally as if it is unconfined. CE-VF-2 is not located near an outcrop, however it one of three nested piezometers and adjacent piezometers may have caused local effects similar to the effect of carbonate-rock outcrops.

Well CE-VF-2 (4.4 percent) yielded the largest estimate of porosity in the carbonate rock aquifers. The site is located along the axis of the White River ground-water flow system, where higher values of porosity might reasonably be expected, but transmissivity for this site is a moderate  $3.0 \times 10^{-3}$  to  $1.1 \times 10^{-2} \text{ m}^2 \text{ s}^{-1}$ . The acoustic- and neutron-density estimates of porosity ( $0.7 \pm 1.1$  percent) are much smaller than the estimate presented here and suggest that one or the other measurement is not right. Site CSV-2 (1.8 percent) has a moderate porosity and moderate transmissivity ( $1.7 \times 10^{-3}$  to  $8.2 \times 10^{-3} \text{ m}^2 \text{ s}^{-1}$ ), however the porosity is smaller than borehole geophysical methods indicate (acoustic density  $4.2 \pm 1.9$  and neutron density  $5.0 \pm 2.0$  percent). Site DDL-2 (2.3 percent) also has a moderate porosity but there are no other data with which to compare the calculations.

## CONCLUSIONS

Aquifer dilatation due to earth-tides and barometric pressure fluctuations may be used effectively to determine storage characteristics and matrix compressibility. The method does not require either removal of water from the well or an observation well. The global theory worked well despite its one-dimensional derivation. The standard form of the global theory slightly overestimates storage terms due to the assumption of incompressible grains. Use of the loading efficiency,  $\alpha^*$ , to accommodate for compression of grains yielded the best results for estimates of both storage characteristics and matrix compressibility.

The soil mechanics theory was used for sites for which an earth tide response was below the detection limits of the equipment and only barometric efficiency could be determined. Calculations based on soil mechanics theory produced estimates of storage characteristics that were similar in range to those estimates by the global theory, but did not match well with site specific data. Aquifer matrix compressibility could not be determined using this method.

Measurement of aquifer dilatation due to earth tides and barometric effects requires aquifers that are at least partially confined. For the carbonate aquifers, the confining layer may in part be located in the unsaturated zone. Also required is a data record covering two months or longer to delineate phase angle and amplitude of the five principle tidal constituents. However, wells that had less than three months' data yielded poor phase-angle resolution. The use of hourly sampling protocol did not allow the static confined barometric efficiency in high-transmissivity ( $10^{-2} \text{m}^2 \text{s}^{-1}$  or more) aquifers to be fully defined, and a more frequent sampling protocol is recommended for such aquifers.

On-site measurement of barometric pressure is preferred, but altitude-corrected barometric pressure from weather stations as far away as 150 kilometers can be used to estimate barometric efficiency (with some loss of accuracy).

Water-level measurements were made with floats and both voltage- and current-signal transducers. Floats are easy to use and produce few calibration errors but have lower resolution (0.3 cm) and can only be used to measure shallow wells. Voltage-signal transducers (0.15 cm resolution) are subject to calibration errors due to voltage and temperature fluctuations but are cheaper than the more reliable amperage-signal transducers. The six-wire voltage-signal configuration was prone to large amounts of drift, which proved troublesome during data reduction.

Matrix compressibility was estimated by an iterative procedure and found to be slightly smaller than initial assumptions. Calculated values range from  $1.05 \times 10^{-11}$  to  $1.35 \times 10^{-11} \text{ Pa}^{-1}$  with an average value of  $1.15 \times 10^{-11} \pm 9 \times 10^{-13} \text{ Pa}^{-1}$ .

Estimates of specific storage for the carbonate aquifers are few, due primarily to the remote access and sparse habitation in the mountainous areas where they crop out. Specific storage in fractured carbonate rocks ranged from  $1.50 \times 10^{-7}$  to  $2.57 \times 10^{-7} \text{ m}^{-1}$ , and average  $2.09 \times 10^{-7} \pm 4.0 \times 10^{-8} \text{ m}^{-1}$  for the wells. Although this is approximately an order of magnitude smaller than expected, it seems reasonable considering the small aquifer matrix compressibility and large amount of compression that actually occurs within the grains themselves. The best estimate of specific storage for Devils Hole is the incompressible grain value of  $4.2 \times 10^{-7} \text{ m}^{-1}$ , and for valley-fill alluvium is  $1.93 \times 10^{-6} \text{ m}^{-1}$ .

---

Table 7 near here

---

The following table shows the results of the regression analysis. The dependent variable is the natural logarithm of the number of employees. The independent variables are the natural logarithm of sales, the natural logarithm of assets, and the natural logarithm of the number of years since the firm was founded. The results show that sales and assets are positively related to the number of employees, while the number of years since the firm was founded is negatively related. The adjusted R-squared is 0.12, indicating that the model explains 12% of the variance in the dependent variable.

Table 7: Regression results for the number of employees. The dependent variable is the natural logarithm of the number of employees. The independent variables are the natural logarithm of sales, the natural logarithm of assets, and the natural logarithm of the number of years since the firm was founded. The results show that sales and assets are positively related to the number of employees, while the number of years since the firm was founded is negatively related. The adjusted R-squared is 0.12, indicating that the model explains 12% of the variance in the dependent variable.

Estimates of storage coefficient range from  $0.63 \times 10^{-5}$  to  $12.08 \times 10^{-5}$ , which is mostly within the range expected. The incompressible grains value of  $1.93 \times 10^{-6} \text{ m}^{-1}$  is considered the best estimate of storage coefficient for the one well in alluvium.

Effective-porosity estimates varied from 1.0 to 3.3 percent for the eastern Nevada carbonate-rock aquifers and the average value was  $1.9 \pm 0.9$ . Effective porosity for valley-fill alluvium was 28.8 percent. The estimates seem reasonable, when interpreted in light of local structure, and specific-capacity and pumping tests, however the values were only about one quarter to half as large as estimates of total porosity derived from neutron-density, and effective porosity derived from acoustic density. The full reason for this discrepancy is unclear, however the analysis presented here measures an average over the entire borehole whereas the geophysical method used segments of the well where the walls were very straight and the geophysical technique relies on estimates of borehole fluid parameters which were not actually measured in the field.

## REFERENCES CITED

- Bear, Jacob, 1972, Dynamics of fluids in porous media: New York, Elsevier, 764 p.
- Bendat, J.S., and Piersol, A.G., 1986, Random data analysis and measurement procedures (2nd ed.): New York, John Wiley and Sons, 566 p.
- Berger, D.L., 1992, Aquifer properties of fractured carbonate rock from selected, drill holes in southern Nevada as interpreted from borehole geophysical logs: U.S. Geological Survey Water Resources Investigations 91-4167, 15p.
- Berger, D.L., and Kilroy, K.C., 1988, Geophysical logs and hydrologic data for eight wells in the Coyote Spring Valley area, Clark and Lincoln Counties, Nevada: U.S. Geological Survey Open-File Report 87-679, 59 p.
- Biot, M.A., 1941, General theory of three-dimensional consolidation: J. Appl. Phys., v.12, p.155-164.
- Bodvarsson, Gunnar, 1970, Confined fluids as strain meters: J. Geophys. Res. v.75, p.2711-2718.
- Bower, D.R., 1983, Bedrock fracture parameters from the interpretation of well tides: J. Geophys. Res. v.88, p.5025-5035.
- Bredehoeft, J.D., 1967, Response of well-aquifer systems to earth tides. J. Geophys. Res., v. 72, p.3075-3087.
- Carmichael, R.S., ed., 1982, Handbook of physical properties of rocks: Boca Raton, Fla., CRC Press Inc., v.2, 345 p.
- Carr, P.A., and Van der Kamp, G.S., 1969, Determining aquifer characteristics by the tidal method: Water-Resour. Res. v.5, p.1023-1031.
- Carroll, M.M., 1979, An effective stress law for anisotropic elastic deformation: J. Geophys. Res. v.72, p.7510-7512.
- Clark, W.E., 1967, Computing the barometric efficiency of a well: J. Hydraul. Eng. v.93, p.93-98.

- Considine, J.A., 1976, The rigid plate model of the barometric effect: *Journal of Hydrology*, v. 7, p. 233-245.
- Cooper, H.H., Jr., 1966, The equations of groundwater flow in fixed and deforming coordinates: *J. Geophys. Res.* v.71, p.4785-4790.
- Cooper, H.H., Jr., Bredehoeft, J.D., Papadopulos, I.S., and Bennett, R.R., 1965, The response of well-aquifer systems to seismic waves: *J. Geophys. Res.* v.70, p. 3915-3926.
- DeWiest, R.J., 1966, On the storage coefficient and the equations of groundwater flow: *J. Geophys. Res.* v.71, p.1117-1122.
- Dennis, R. E., and Long, E. E., 1971, A user's guide to a computer program for harmonic analysis of data at tidal frequencies: Rockville, Md. National Oceanic and Atmospheric Administration Technical Report 41, 31 p.
- Freeze, R.A., and Cherry, J.A., 1979, *Groundwater*: Englewood Cliffs, New Jersey, Prentice Hall, Inc., 604 p.
- Galloway, Devin, and Rojstaczer, S.A., 1989, Analysis of the frequency response of water levels in wells to earth tides and atmospheric loading: *Proceedings of the 4th Canadian/American Conference on hydrogeology: Fluid flow, heat transfer, and mass transfer in fractured rocks*, ed. B. Hitchon, S. Bachu, C. Sauveplane, Alberta Research Council, Edmonton Alberta, pub. NWWA, Dublin, OH, p. 100-113.
- Gilliland, J. A., 1969, A rigid plate model of the barometric effect: *J. Hydrology* v.7, p.233-245.
- Godin, G., 1972, *The analysis of tides*: Buffalo, New York, University of Toronto Press, 264 p.
- Hanson, J.M., 1984, Evaluation of subsurface fracture geometry using fluid pressure response to solid earth tidal strain: Lawrence Livermore National Laboratory Report UCID-20156, 135 p.
- Hantush, M.S., 1964, *Hydraulics of wells*: *Adv. Hydrosci.* v.1 p.281-432.

- Hoffman, R.J., 1989, Chronology of diving activities and underground surveys in Devils Hole, and Devils Hole Cave, Nye County, Nevada, 1950-86: U.S. Geological Survey Open-File Report 88-93, 12 p.
- Hsieh, P.A., Bredehoeft, J.D., and Farr, J.M., 1987, Determination of aquifer transmissivity from earth tide analysis: Water Resources Res. v.23, p.1824-1832.
- Jacob, C.E., 1941, On the flow of water in an elastic artesian aquifer: Eos Amer. Geophys. Union Trans. v.27, p.574-586.
- Lindburg, P.E., 1982, Engineer in training review manual: San Carlos, Calif., Professional Publications, 411 p.
- Love, A.E.H., 1926, A treatise on the mathematical theory of elasticity: New York, Ny, Dover, 643 p.
- Longman, I. M., 1959, Formulas for computing the tidal accelerations due to the Moon and the Sun: J. Geophys. Res. v.64, p.2351-2355.
- Marine, I. W., 1975, Water level fluctuations due to earth tides in a well pumping from slightly fractured crystalline rock: Water Resources Res. v.11, p.165-173.
- Melchior, Paul, 1956, Sur l'effet des marees terrestres dans les variations de niveau observees dans les puits et particulier au sondage de Turnhout: Belgium, Commun. Obs. Roy. Belgique. v.108, p.7-28.
- Melchior, Paul, 1960, Die Gezeiten in unterirdischen Flussigkeiten: Erdoel Kohle v.13, p.312-317.
- Melchior, Paul, 1983, The tides of the planet earth: New York, NY, Pergamon Press, 641p.
- Muller, D.C., and Kibler, J.E., 1984, Preliminary analysis of geophysical logs from drill hole UE-25p#1, Yucca Mountain, Nye County, Nevada: U.S. Geological Survey Open-File Report 84-649, 14 p.
- Munk, W.H., and MacDonald, G.J.F., 1960, The rotation of the earth: Cambridge University Press, Cambridge, England 323 p.

- Narasimhan, T.N., and Kanehiro, B.Y., 1980, A note on the meaning of storage coefficient: *Water Resour. Res.* v.14, p.423-429.
- Narasimhan, T.N., Kanehiro, B. Y., and Witherspoon, P. A., 1984, Interpretation of earth-tide response of three deep, confined aquifers: *J. Geophys. Res.* v.89, p. 1913-1924.
- Nur, Amos, and Byerlee, J.D., 1971, An exact effective stress law for elastic deformation of rock with fluids: *J. Geophys. Res.* v.76, p.6414-6419.
- Palciauskas, V.V., and Domenico P.A., 1989, Fluid pressures in deforming porous rocks: *Water Resources Res.* v. 25, no.2, p.203-213.
- Rhoads, G.H., Jr., and Robinson, E.S., 1979, Determination of aquifer parameters from well tides: *J. Geophys. Res.* v.84, p.6071-6082.
- Rice, J.R., and Cleary, M.P., 1976, Some basic stress diffusion solutions for fluid-saturated porous media with compressible constituents: *Rev. Geophys. Space Phys.* v.14, p.227-241.
- Robinson, E.S., and Bell, R.T., 1971, Tides in confined well aquifer systems: *J. Geophys. Res.* v.76, p.1857-1869.
- Rojstaczer, S., 1988A, Determination of fluid flow properties from the response of water levels in wells to atmospheric loading: *Water Resources Res.* v.24, no.11, p.1927-1938.
- Rojstaczer, S., 1988B, Intermediate period response of water wells to crustal strain: sensitivity and noise level: *J. Geophys. Res.* v. 93, p.13619-13634.
- Rojstaczer, S., and Agnew, D.C., 1988, The influence of formation material properties on the response of water levels in wells to earth Tides and atmospheric loading: *J. Geophys. Res.* v. 94, p. 12403-12411.
- Rouse, Hunter, ed., 1950, *Engineering hydraulics*: New York, NY, John Wiley and Sons, 1039 p.
- Rush, F.E., 1968, Index of hydrographic areas of Nevada: *Nev. Div. Water Res. Water Resources Investigations Report 6*, 38 p.

- Schaefer, D.H., Morris, T.M., and Dettinger, M.D., (in press)  
Hydrologic and geophysical data for selected wells and springs in  
the Sheep Range area, Clark and Lincoln Counties, Nevada: U.S.  
Geological Survey Open-File Report 89-425.
- Schureman, P. W., 1941, Manual of harmonic analysis and prediction of  
tides (revised edition): Washington D.C., U. S. Department of  
Commerce, Coast and Geodetic Survey Special Publication 98, 400 p.
- Skempton, A.W., 1954, The pore-pressure coefficients A and B:  
Geotechniques v.4, p.143-147.
- Theis, C.V., 1935, The relation between lowering of the piezometric  
surface and the rate and duration of discharge of a well using  
groundwater storage: EOS American Geophys Union Trans., p.519-524.
- Van der Kamp, G. and Gale, J.E., 1983, Theory of earth tide and  
barometric effects in porous formations with compressible grains:  
Water Resources Res. v.19, p.538-544.
- Weeks, E. P., 1979, Barometric fluctuations in wells tapping deep  
unconfined aquifers, Water Resources Res. v.15, p.1167-1176.

## NOTATION

- A is water level amplitude (length).
- An is the sum over the interval 0 to x of h(t) (length).
- Ap(t) is the moving average at time t (length).
- a is mean earth radius (length).
- b is a trigonometric residual (dimensionless).
- BE is barometric efficiency, the ratio of water-level change to barometric pressure head change (dimensionless).
- BE' is static confined barometric efficiency (dimensionless).
- dha is hydraulic head in the aquifer (length).
- dha' is hydraulic head in the aquifer due to barometric effects (length).
- dhb is barometric pressure head (length).
- dhw is water level in a well (length).
- dhw' is water level in a well due to barometric pressure effects (length).
- dhw'\* is water level in a well due to barometric pressure effects that has been compensated for small phase shifts (length).
- dhw'' is water level in a well due to earth-tide effects (length).
- D' is the amplitude of the tidal wave relative to the maximum lunar tide (length).
- f is frequency (radians day<sup>-1</sup>).
- g is acceleration due to gravity (length time<sup>-2</sup>).
- h is a Love number (dimensionless).
- h(t) is pressure head at time t (length).
- H is the difference in altitude between a weather station and a site where barometric pressure is estimated (length).
- J is a trigonometric coefficient (dimensionless).
- K is a trigonometric coefficient (dimensionless).
- L is the dry adiabatic lapse rate (degrees length<sup>-1</sup>).
- n is porosity (dimensionless).

- $P_o$  is barometric pressure at a weather station (mass length<sup>-1</sup>time<sup>-2</sup>).  
 $P_s$  is estimated barometric pressure (mass length<sup>-1</sup>time<sup>2</sup>).  
 $R$  is the Universal gas constant (mass length<sup>2</sup>time<sup>-2</sup>degrees<sup>-1</sup>).  
 $S$  is storage coefficient (dimensionless).  
 $S_s$  is specific storage (length<sup>-1</sup>).  
 $S_y$  is specific yield (dimensionless).  
 $TE$  is tidal efficiency (dimensionless).  
 $T_o$  is the temperature at a weather station (degrees).  
 $t$  is time (hours).  
 $tt$  is travel time recorded by the acoustic log (time length<sup>-1</sup>).  
 $tf$  is travel time in the fluid (time length<sup>-1</sup>).  
 $tm$  is travel time in the rock matrix (time length<sup>-1</sup>).  
 $V_a$  is aquifer volume (length<sup>3</sup>).  
 $W_2$  is tide generation potential (area time<sup>-2</sup>).  
 $W_{2d}$  is diurnal tide generation potential (area time<sup>-2</sup>).  
 $W_{2s}$  is semidiurnal tide generation potential (area time<sup>-2</sup>).  
 $x$  is window size for the moving average operator (dimensionless).  
 $Z$  is the maximum lunar-tide amplitude (length).  
 $\alpha$  is the fraction of the rock strain accomodated by the grains (dimensionless).  
 $\alpha^*$  is the fraction of the rock strain accomodated by the grains derived from definition equations for compressibility (dimensionless).  
 $\beta$  is aquifer matrix compressibility (length time<sup>2</sup>mass<sup>-1</sup>).  
 $\beta_l$  is compressibility of the liquid water (length time<sup>2</sup>mass<sup>-1</sup>).  
 $\beta_p$  is compressibility of the pores, drained (length time<sup>2</sup> mass<sup>-1</sup>).  
 $\beta_s$  is compressibility of the solid material (length time<sup>2</sup>mass<sup>-1</sup>).  
 $\Delta_a$  is aquifer dilatation (dimensionless).

- $\Delta e$  is aquifer dilatation due to earth tides (dimensionless).
- $\Delta e^*$  is aquifer dilatation due to earth tides compensated for small phase lags (dimensionless).
- $\nu$  is Poisson's ratio, a constant of proportionality (dimensionless).
- $\rho$  is density of water (mass length<sup>-3</sup>).
- $\rho_b$  is bulk density of the aquifer (mass length<sup>-3</sup>).
- $\theta$  is the colatitude (90 minus the latitude, in degrees)
- $\phi_e$  is the phase angle between the tide generation potential and the earth-tide dilatation (degrees).
- $\phi_t$  is the phase angle between the tide generation potential and the 0 meridian in Greenwich England (degrees).
- $\phi_w$  is the phase angle between the tide generation potential and the water level oscillation due to earth-tide dilatation (degrees).
- $\phi_w''$  is the phase angle between the tide generation potential and the water level oscillation due to earth-tide dilatation corrected for offset from the principal meridian (degrees).

## APPENDICIES

Appendix A Neutron-Density Estimation Of Porosity

Neutron-density cross-plots are used to estimate porosity in impure carbonate rocks. The method requires information from several different borehole logs to work successfully. Geologic logs are used to define gross lithology, based on chips brought out of the hole along with drilling mud. A caliper log is used to identify sections of the borehole which are smooth and round. This is necessary because interpretation of all other logs is based on an assumption of constant distance between the probe and bore wall. A gamma-gamma log is used to measure bulk density,  $\rho_b$ . The tool emits gamma radiation from a cesium-137 source and measures radiation backscattered by electrons in the adjacent rocks. An inverse relationship exists between detected radiation and bulk density. A natural-gamma log is used to identify shaley units. The natural-gamma probe measures the concentration of naturally occurring gamma radiation produced principally by radioactive decay of potassium 40, uranium 238, and thorium 232. These elements are especially concentrated in clays and shales. Identification of clays and shales is important to interpretation of the neutron log. The neutron probe emits neutrons from an americium-berillium source that react sparingly with larger atoms but are slowed down by hydrogen atoms. An inverse relationship exists between the number of neutrons counted by the detector and the amount of hydrogen in the formation. The main sources of hydrogen in a carbonate rock are water held in pore spaces, and clay minerals, hence the need to identify clays with the natural gamma log. A calibration equation is used to convert the neutron response to apparent porosity. A correction is also applied for clay rich zones.

A number of smooth-bore, saturated zones are identified from the logs for the estimation of porosity. For these zones, the average bulk density, measured directly by the gamma-gamma log, against average apparent porosity are plotted along with type curves for pure

limestone, dolomite, and silica. Zones that do not plot directly on the type curves indicate a deviation from pure lithology assumed in the neutron response calibration equation. The true porosity is interpolated from the graph. See figure 8 for well CE-DT-4.

#### Appendix B Acoustic Density Estimation Of Porosity

For wells in which a neutron log is not available, total porosity can be estimated using the acoustic-density cross plot. An acoustic probe measures the transit time required for an acoustic pulse to travel a specified distance through the formation. A calibration equation is used to determine apparent porosity from the log.

$$t_t = t_f n + (t_m (1-n)), \quad (53)$$

where,

$t_t$  is travel time recorded by the acoustic log ( $\mu\text{sec m}^{-1}$ ).

$t_f$  is travel time in the fluid ( $656\mu\text{sec m}^{-1}$ ),

$t_m$  is travel time in the rock matrix ( $131\mu\text{sec m}^{-1}$ )

$n$  is porosity (dimensionless).

The true porosity is interpolated from a plot of bulk modulus against apparent porosity with type curves. See figure 9 for well CE-DT-6. Unfortunately, the acoustic log is not as accurate as the neutron log for determining apparent porosity because acoustic waves tend to travel around fractures and underestimate porosity. When the acoustic waves travel across fractures, cycle skips may occur where the first arrival of an acoustic signal is missed, leading to an overestimation of apparent porosity.

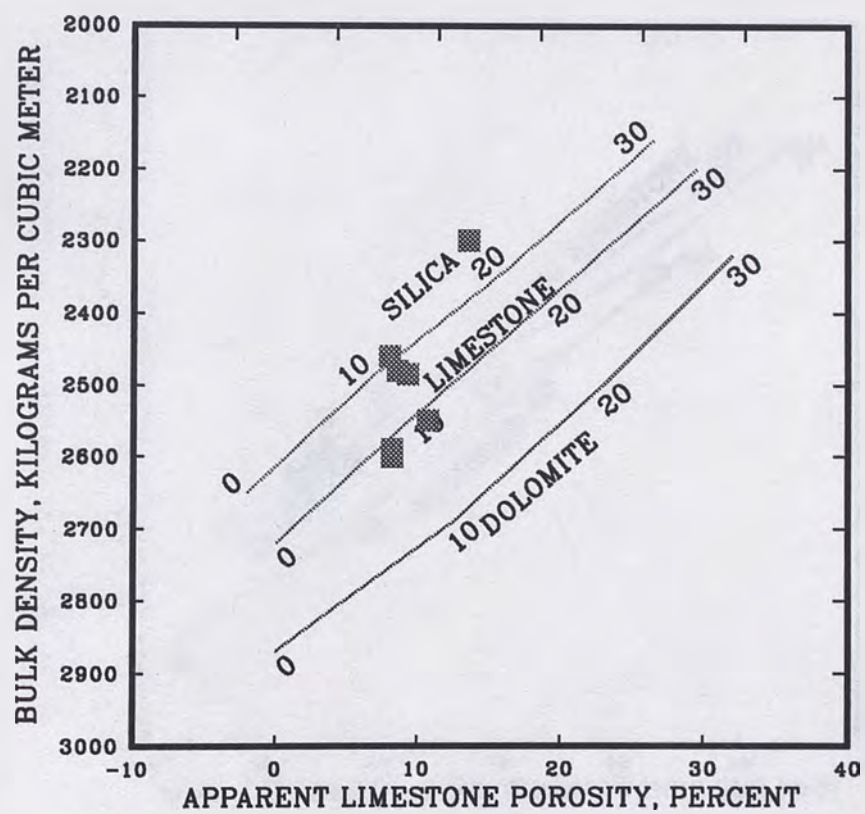


Figure 10.--Neutron-density cross plot for seven zones of well CE-DT-4

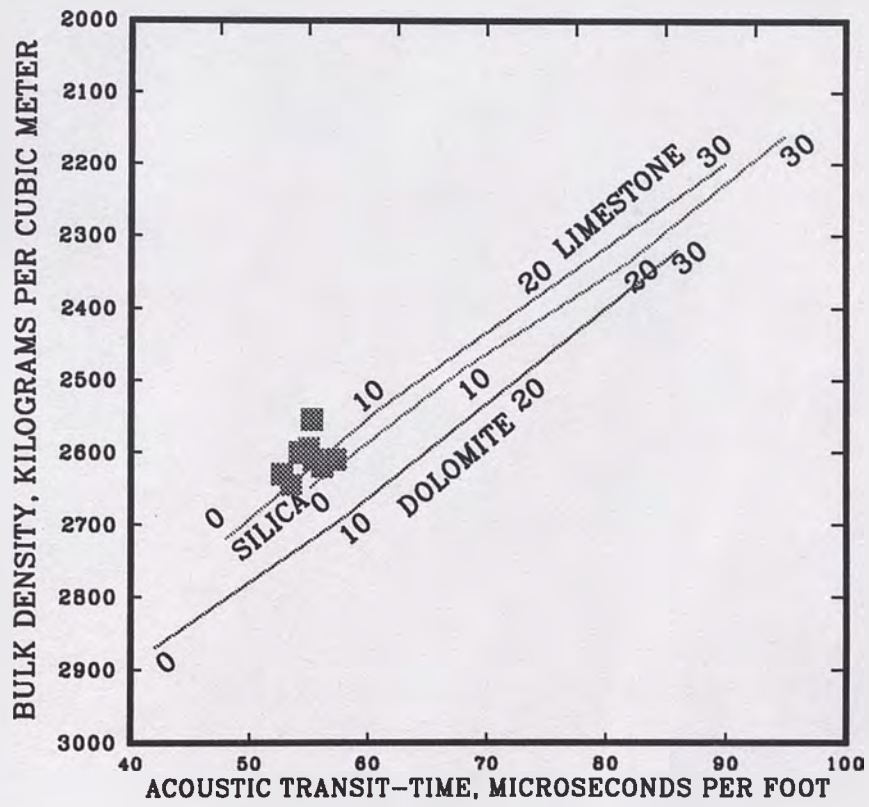


Figure 11.--Acoustic-density cross plot for eight zones of well CE-DT-4.